NACELLE AERODYNAMIC AND INERTIAL LOADS (NAIL) PROJECT FINAL TECHNICAL REPORT

ENERGY EFFICIENT TRANSPORT PROGRAM

BOEING COMMERCIAL AIRPLANE COMPANY
P. O. BOX 3707, SEATTLE, WA 98124

NASA

FOREWORD

This report presents a description, principal results, and analysis of the Nacelle Aerodynamic and Inertial Loads (NAIL) project. The work was conducted under NASA contract NAS1-15325 from October 1979 through August 1981. The contract was managed by the NASA Energy Efficient Transport Office (EETPO), headed by Mr. R. V. Hood, which is a part of the Aircraft Energy Efficiency (ACEE) program organization at the Langley Research Center. Mr. D. B. Middleton and Mr. K. W. Heising were the technical monitors for the contract. The work was performed in the Engineering and the Flight Operations organizations of the Boeing Commercial Airplane Company. Key contractor personnel responsible for the material in this report were:

G. W. Hanks
Program Manager

R. L. Martin
Project Manager

K. H. Dickenson
Structures Technology

W. F. Wilson
Flight Test Operations

W. R. Lambert
Propulsion Technology

L. I. Tolle
Propulsion Technology

F. J. Davenport
Structures Technology

P. G. Kafka
Structures Technology

E. L. Wallace
Flight Test Analysis

J. P. Falatko
Flight Test Analysis

B. W. Farquhar
Propulsion Technology

B. K. Hodder
Propulsion Technology

F. W. McIlroy
Flight Test Instrumentation

C. D. Beard
Flight Test Instrumentation

R. D. LaBounty
Industrial Engineering Flight Test Support

B. G. Skelton
Flight Test and Crew Training Support

The test effort was conducted in cooperation with the Pratt & Whitney Aircraft Group, which was supported by the NASA-Lewis Research Center under contract NAS3-20632.

CONTENTS

CONTENTS

FIGURES

FIGURES

TABLES

1.0 SUMMARY

The Nacelle Aerodynamic and Inertial Loads (NAIL) project consisted of two distinct tasks. They were the flight loads study and the installed propulsion system aerodynamics (IPSA) study.

1.1 FLIGHT LOADS

The NAIL flight loads study comprised a series of flight tests to measure the aerodynamic and inertial loads imposed on the Pratt & Whitney JT9D-7 turbofan engines of a Boeing 747 airplane under conditions of flight acceptance testing and of typical revenue service. Aerodynamic loads were determined by integrating pressures measured at 252 locations on the right-hand inboard engine inlet and fan cowl. The relative load level on the right-hand outboard engine was established by 45 pressure measurements, which were compared with the corresponding inboard engine pressures. Inertial loads were determined by sets of linear accelerometers mounted on the engines and inlets, and also on the wing at the nacelle strut attach points, and by rate gyros mounted on the engine fan cases.

The purpose of the measurements was to clarify the influence of flight loads on engine performance deterioration due to enlarged rotor tip clearances caused by the rotor rubbing on the engine case under load. Rotor/case clearances were measured in flight by laser probes mounted on the fan and high-pressure turbine case of the inboard engine and on the fan case of the outboard engine. Airplane flight condition data and engine performance data were measured and recorded for all flight conditions. (This document deals with the measured flight loads. Correlation of these loads with clearance changes and analysis of engine performance effects is reported separately in refs. 1 and 2.) Aerodynamic and inertial loads were estimated prior to flight test (ref. 3).

Inlet aerodynamic pitching moments were measured for a group of flight conditions typical of a transport mission and for a group of conditions characteristic of a 747 acceptance test flight. It was found that:

● The severest operating airloads occur during takeoffs.

● Airloads were generally larger than estimated while inertial loads were smaller.

● Calculations based on measured inlet airload sensitivity to change in angle of attack show that transient inlet airloads due to gusts are considerably smaller than takeoff airloads.

● Airloads can be significantly reduced by revisions to flight procedures.

The pressure data were also tabulated in computer data files suitable for finite-element analyses of engine/nacelle structures and provided to Pratt & Whitney for correlation of measured and calculated clearance changes. (This effort will be reported separately by Pratt & Whitney.)

To permit application of the NAIL loads data to aircraft/engine combinations other than the 747/JT9D, the vertical force and pitching moments at high angle of attack and airflow were expressed as aerodynamic coefficients and correlated with estimated inlet angle of attack and nondimensional engine airflow. The resulting expressions can be used to estimate inlet airloads for any roughly similar inlet geometry, provided the inlet angle of attack is known.

1.2 INSTALLED PROPULSION SYSTEM AERODYNAMICS (IPSA)

The IPSA portion of the NAIL project created a data base of pressures measured on the inlets, cowls, struts, and adjacent wing surfaces of the two right-hand engines of a Boeing 747. These data, along with the aerodynamic geometry definition, will be used to develop and verify analytical flow models and computer codes to be employed in the design of propulsion system aerodynamic configurations having reduced interference drag.

In the course of three test flights, pressure data were obtained for Mach numbers 0.77, 0.80, 0.86, and 0.91 at lift coefficients corresponding to cruising flight.

2.0 INTRODUCTION

2.1 BACKGROUND

2.1.1 Flight Loads

Since the introduction of the jet engine into commercial transport service, historical data have indicated that deterioration of engine thrust specific fuel consumption (TSFC) occurs over the life of installed engines. When fuel was cheap and plentiful, increases in TSFC were merely a nuisance rather than a technical problem requiring a solution. But the shortages and price increases following the 1973 oil embargo made TSFC increases a serious issue. Accordingly, the NASA Engine Component Improvement (ECI) program (part of the NASA Aircraft Energy Efficiency program) was made responsible for determining the cause of and potential solutions to installed engine TSFC deterioration. As part of the ECI program, Boeing Commercial Airplane Company (BCAC) assisted Pratt & Whitney (P&WA) under NASA-Lewis contract in an investigation of this problem (ref. 3).

It was found that early deterioration was due primarily to rotor blade tips rubbing against the engine casing as the engine deformed under its operating loads. This rubbing caused increased clearances and gas flow leakage, resulting in a cruise TSFC deterioration of about 0.8% after the predelivery acceptance testing and an additonal 0.3% in 2000 flights in revenue service.

Factors contributing significantly to engine performance losses are divided into engine loads and flight loads.

- Engine loads are those not related to the flight environment:
    - Internal engine pressures
    - Thermal loads due to temperature differentials
    - Thrust loads—fore and aft
    - Centrifugal loads

- Flight loads are those imposed by the flight environment:
    - Aerodynamic pressures
    - Inertial forces

Engine deformation calculations made with a finite-element mathematical model of the engine/nacelle structure indicated that 87% of the TFSC deterioration in the first 1000 flights was due to aerodynamic flight loads. Long-term deterioration (after 1000 flights) was ascribed mainly to thermal loads and to blade profile changes caused by erosion.

The aerodynamic loads causing engine deformation act mainly on the inlet, which is attached to the fan case. The inlet airloads used for the deformation estimate were derived from a very limited data base. Scale effects cast doubt on small-scale wind tunnel load and pressure measurements, while the full-scale data available at the time were very sketchy both with respect to flight conditions and to geometric coverage.

It was concluded that a new experimental program was needed to measure in flight both the loads and the associated clearance changes. A feasibility study of a flight program was made and reported in reference 4. Subsequently, NASA-Langley and NASA-Lewis Research Centers authorized and jointly funded this program under separate contracts with BCAC and P&WA. The BCAC effort, the Nacelle Aerodynamic and Inertial Loads

3

(NAIL) project, was funded by NASA-Langley and NASA-Lewis under task 4.3 of contract NAS1-15325. The P&WA effort was funded by NASA-Lewis.

2.1.2 Installed Propulsion System Aerodynamics (IPSA)

The installation of propulsion systems on aircraft wings causes a drag increment called interference drag. This increment is the difference between the drag of the aircraft with the propulsion system installed and the sum of the drag of the isolated aircraft plus the drag of the isolated propulsion system. Interference drag results from a combination of flow processes near the nacelle, wing, and pylon. It includes effects of local circulation changes about the wing due to the propulsion system, of shock waves that form between the wing and nacelle, and of boundary layer flows separating from the nacelle, pylon, and the underside of the wing. Historically, studies of propulsion system interference drag have been confined to exploratory tests in wind tunnels that allowed variation of only a few of the many parameters involved. Now, numerical solutions are being developed for the governing equations of transonic flow about three-dimensional bodies. A comprehensive data base of the flow properties around a propulsion system installed near a wing was needed to validate the analytical results and to uncover modeling inadequacies.

The NAIL flight loads program, already authorized and underway, provided instrumentation capable of measuring a substantial portion of the pressures needed for the Installed Propulsion System Aerodynamics (IPSA) study. It was logical and economical to expand the scope of NAIL to include IPSA, and contract NAS1-15325, between NASA-Langley Research Center and BCAC, was revised accordingly.

2.2 OBJECTIVES

The objectives of the flight test program were to:

- Measure flight loads (aerodynamic and inertial) typical of the production acceptance flight (a substantial contributor to short-term deterioration) and revenue service flights

- Explore the effects of gross weight, pitch and yaw rate, touchdown sink rate, and various maneuvers on nacelle loads

- Measure simultaneously engine clearance closures and engine performance changes

- Provide a data base for designing improved propulsion systems (performance retention)

- Provide a data base of pressures measured on wing, pylon, and nacelle surfaces of both inboard and outboard propulsion installations of commercial transport-sized aircraft and gather information on airflow patterns surrounding the powerplant installations using static pressure surveys

2.3 APPROACH

A 15-hour flight test program covering the entire acceptance flight profile, variations in takeoff and landing conditions, and high-g turns was defined to measure simultaneously the flight loads (cause) and engine clearance changes (effect) associated with engine performance deterioration.

4

The testing was conducted on the Boeing-owned 747 RA001 test bed airplane during the concurrent JT9D-7R4 engine development program for the Boeing 767 airplane. Following a functional check flight conducted from Boeing Field International on 3 October 1980, the airplane and test personnel were ferried to Valley Industrial Park near Glasgow, Montana on 7 October 1980. The combined NAIL and 767/JT9D-7R4 test flights were conducted at the Glasgow remote test site, and the airplane was returned to Seattle on 26 October 1980. (As a result of the two programs being conducted in parallel, the NAIL program benefited from more than 33 hr of flight test and included more flight conditions than originally planned.)

Inertial loads were measured by six accelerometers and two rate gyros on both right-hand engines. The pylon and strut interface on both engines was equipped with an additional six accelerometers. The engine clearance changes were measured by laser proximity probes on the fan of both engines and on the high-pressure turbine of the inboard engine. Engine performance instrumentation and 20 high-pressure turbine thermocouples provided additional data on the inboard engine for resolving clearance and performance changes.

Aerodynamic loads were measured by integrating pressures measured at 252 taps on the right-hand inboard nacelle. Loads for the right-hand outboard nacelle were monitored by comparing pressures measured at 45 taps to those measured at corresponding locations on the inboard nacelle.

IPSA pressures were measured on both of the right-hand pylons and core cowls and on the adjacent wing surfaces. In addition, pressures measured at a large number of the taps installed for the flight loads effort (located on the inlet and fan cowl) were applicable to IPSA. A total of 557 pressure measurements were obtained for each IPSA flight condition.

NOTE:

Certain commercial materials are identified in this paper in order to specify adequately which materials were used in the research effort. In no case does such identification imply recommendation or endorsement of the product by NASA or Boeing, nor does it imply that the materials are necessarily the only ones available for the purpose.

3.0 SYMBOLS AND ABBREVIATIONS

$A_{(\ )}$	acceleration in direction indicated by subscript ( )
AC	axial acceleration
ACCEL	acceleration
ADAMS	airborne data analysis and monitor system
A-flange	engine front flange (at nacelle station 100)
AFP	airflow parameter
A_H	inlet highlight area
BCAC	Boeing Commercial Airplane Company
CAS	calibrated airspeed
CG	center of gravity
$C_{F(\ )}$	inlet force coefficient in direction indicated by subscript ( )
C_L	airplane lift coefficient
$C_{M(\ )}$	inlet moment coefficient about axis indicated by subscript ( )
C_P	pressure coefficient
EAS	equivalent airspeed
ECI	Engine Component Improvement program
EPR	engine pressure ratio
E3	engine position 3
E4	engine position 4
FT	flight test
$F_{(\ )}$	force in direction indicated by subscript ( )
g	acceleration of gravity
GW	airplane gross weight
H_p	pressure altitude
HPT	high-pressure turbine

IGE	in-ground effect
IPSA	installed propulsion system aerodynamics
IRIG	inter-range instrumentation group master clock
kcas	knots calibrated airspeed, indicated airspeed corrected for position error (calibrated airspeed equals true airspeed in standard atmosphere at sea level)
ℓ_{IN}	inlet length
LH	left hand
M	Mach number
M_∞	freestream Mach number
M_c	design cruise Mach number
M_D	design dive Mach number
$M_{(\ )}$	moment about axis indicated by subscript ( )
n_z	load factor in z direction
NAC STA	nacelle station
NAIL	Nacelle Aerodynamics and Inertial Loads project
NASA	National Aeronautics and Space Administration
NASTRAN	NASA structural analysis
N_1	engine low-pressure rotor speed
N_2	engine high-pressure rotor speed
OGE	out-of-ground effect
P	pressure
P&WA	Pratt & Whitney Aircraft Group, Commercial Products Division
P_{T_2}	total pressure at engine face
q, Q	dynamic pressure, $\frac{1}{2} \rho V^2$

RA001	Boeing-owned 747-100 research aircraft 1
RH	right hand
rms	root mean square
RWA	referred engine airflow, $WA\sqrt{\theta_{T_2}/\delta_{T_2}}$
S	arc length along surface from highlight
S_{nom}	nominal arc length along surface
SLS	sea level standard
TO	takeoff
TR	thrust reverse
TSFC	thrust specific fuel consumption
T_{T_2}	total temperature at engine face
V	true airspeed
V_C	design cruise speed
V_S	stalling speed or the minimum steady flight speed at which airplane is controllable
WA	engine airflow
WBL	wing buttock line
W_f	fuel flow rate
x	vertical coordinate, positive up (see fig. 20)
y	spanwise coordinate, positive inboard (see fig. 20)
z	axial coordinate, positive aft (see fig. 20)
α	angle of attack
α_{IN}	inlet angle of attack
β_{IN}	inlet sideslip angle

δ_{T_2} total pressure ratio at engine face, P_{T_2}/P_{SLS}

θ circumferential angle

θ_{T_2} total temperature ratio at engine face, T_{T_2}/T_{SLS}

ρ air density

4.0 TEST DESCRIPTION AND RESULTS

4.1 TEST DESCRIPTION

The Nacelle Aerodynamic and Inertial Load (NAIL) program consisted of two distinct efforts: the flight loads test and the installed propulsion system aerodynamics (IPSA) test. Both tests were conducted concurrently with the unrelated JT9D-7R4 nacelle and engine development test program on the Boeing-owned 747 RA001 airplane (fig. 1). Separate data collection systems were used, although substantial portions of the flight loads data applied also to IPSA. Airplane and engine performance data applicable to both tests were gathered from instrumentation and data acquisition systems already available in RA001.

Figure 1. RA001 Test Airplane

4.1.1 Test Vehicle

The 747 RA001 airplane is the first Boeing 747 airframe built and has been used in company flight programs continuously since 1969. It is a model 747-100 and, as such, is limited to a maximum takeoff gross weight of 317.5t (700 000 lb). For these tests, RA001 was limited to a maximum normal load factor of 2.0g flaps up, and 1.6g flaps extended.

4.1.1.1 Flight Loads

The right-hand inboard engine position ("No. 3"), was chosen for greater emphasis because slightly more severe loads were expected at the inboard location and position 2 was not available. A JT9D-7A engine, serial no. P662204, was returned to the P&WA facility and "analytically rebuilt" with new rubstrips, seals, and carefully measured clearances. In addition, it was fitted with a specially built turbine case equipped with laser proximity

11

probes, while another set of laser proximity probes was installed in the fan case. Its performance was then calibrated in a test stand. After return shipment to BCAC, this engine was fitted with an inlet containing comprehensive pressure measuring instrumentation and installed in position 3 on RA001 (fig. 2). Following the flight program, engine P662204 was returned to P&WA for further static testing, followed by "analytical teardown" (with careful inspection of parts and measurement of clearances) and refurbishment. Engine 4, the right-hand outboard engine, was fitted with a fan case rebuilt at P&WA containing a set of laser proximity probes and an inlet with enough pressure instrumentation to determine airloads relative to engine 3.

4.1.1.2 Installed Propulsion System Aerodynamics (IPSA)

Description of the 747 test vehicle, for the purposes of the IPSA program, requires geometrical definitions of the fan inlet, fan cowl, pylon, and core cowl for an inboard and an outboard engine installation. It also requires neighboring wing geometry for each engine. All such required geometry data, defined by relative positions and contours of pressure orifice rows and wing-pylon, pylon-nacelle intersections, is provided in reference 5, section 4.1.1.2.

4.1.2 Instrumentation

The NAIL program was an ambitious undertaking in terms of number of measurements obtained. There were 693 pressure ports, 30 accelerometers, 7 rate gyros, 12 blade clearance measurements, and 20 thermocouples for required test data. Numerous thermocouples were used to provide temperature information on heat-sensitive instrumentation. Finally, expanded engine performance data were provided by an additional 68 measurement channels. The quantity and quality of the data obtained were excellent.
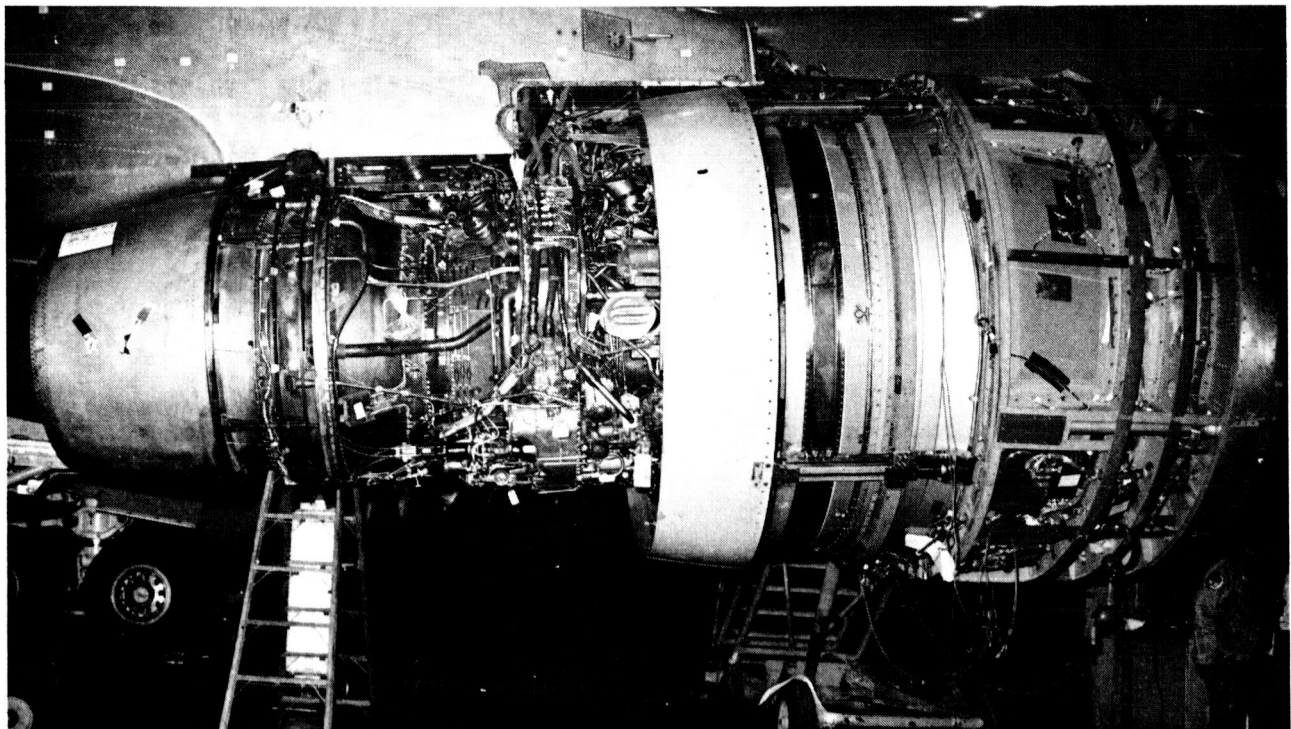
Figure 2. Inboard Engine Buildup

12

Instrumentation placed on or near the numbers 3 and 4 engine and pylon was designed to further the understanding of the flight loads (cause) and engine clearance changes (effect) associated with engine deterioration and to provide information on the flight environment of the engine and wing interface.

4.1.2.1 Flight Loads

Pressure Instrumentation—Most of the pressure instrumentation was placed on the inlet of engine 3 (figs. 3, 4, and 5). It was believed that the inboard engine was subject to higher angles of attack than the outboard engine because wing bending reduced the incidence of the outboard nacelle and because the outboard nacelle was less affected by upflow induced by the wing flaps. Therefore, the inboard nacelle sustained greater loads and was chosen for a more detailed survey using 252 pressure taps.
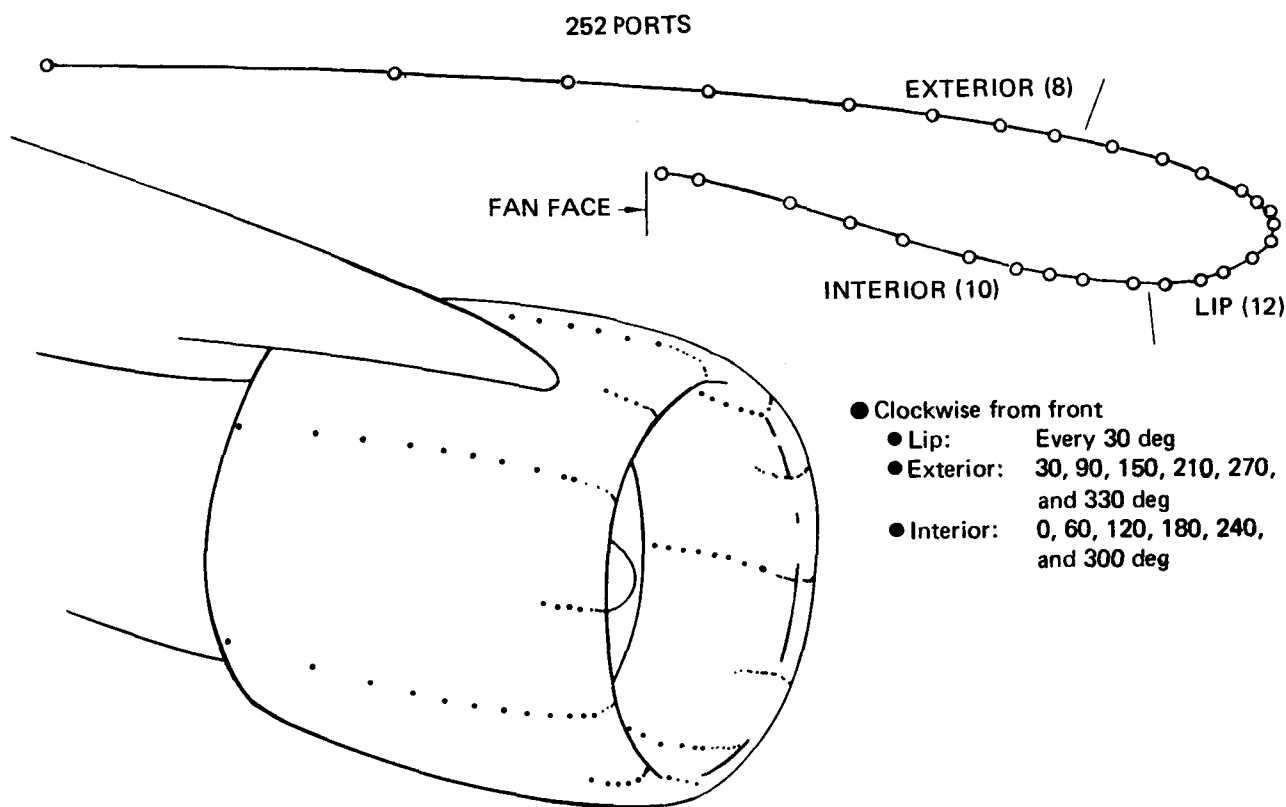
Figure 3. Inboard Engine Pressure Taps

The greatest deviations from ambient pressure and most rapid variations of pressure with distance occur near the inlet lip. The contribution of the lip area to the overall force and moment is very large. Because of this contribution, 144 taps in 12 rows, 30 deg apart, were located in the lip area. Aft of the lip, 60-deg circumferential spacing of the rows provided adequate definition.

Each pressure tap was connected to an Endevco pressure transducer (fig. 6) by approximately 2.44m (8 ft) of 0.155 cm (0.061 in) inside diameter copper tubing to ensure that lag effects were equalized. The transducers were mounted in temperature controlled boxes in groups of 22 (figs. 7 and 8). Each transducer measured differential pressure between the tap and a reference pressure.

13
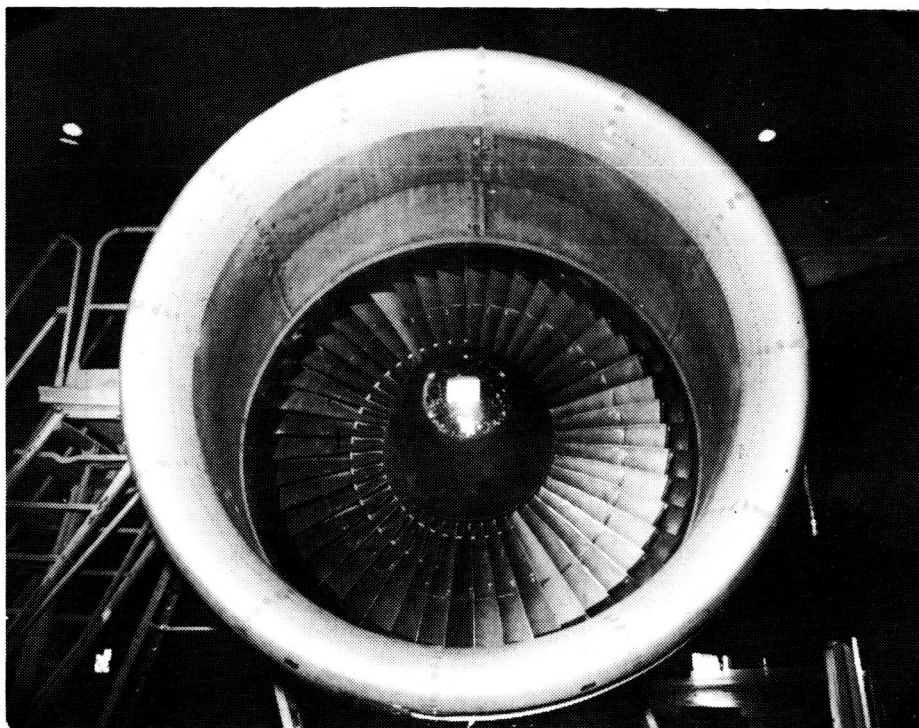
Figure 4. Inboard Inlet Pressure Taps
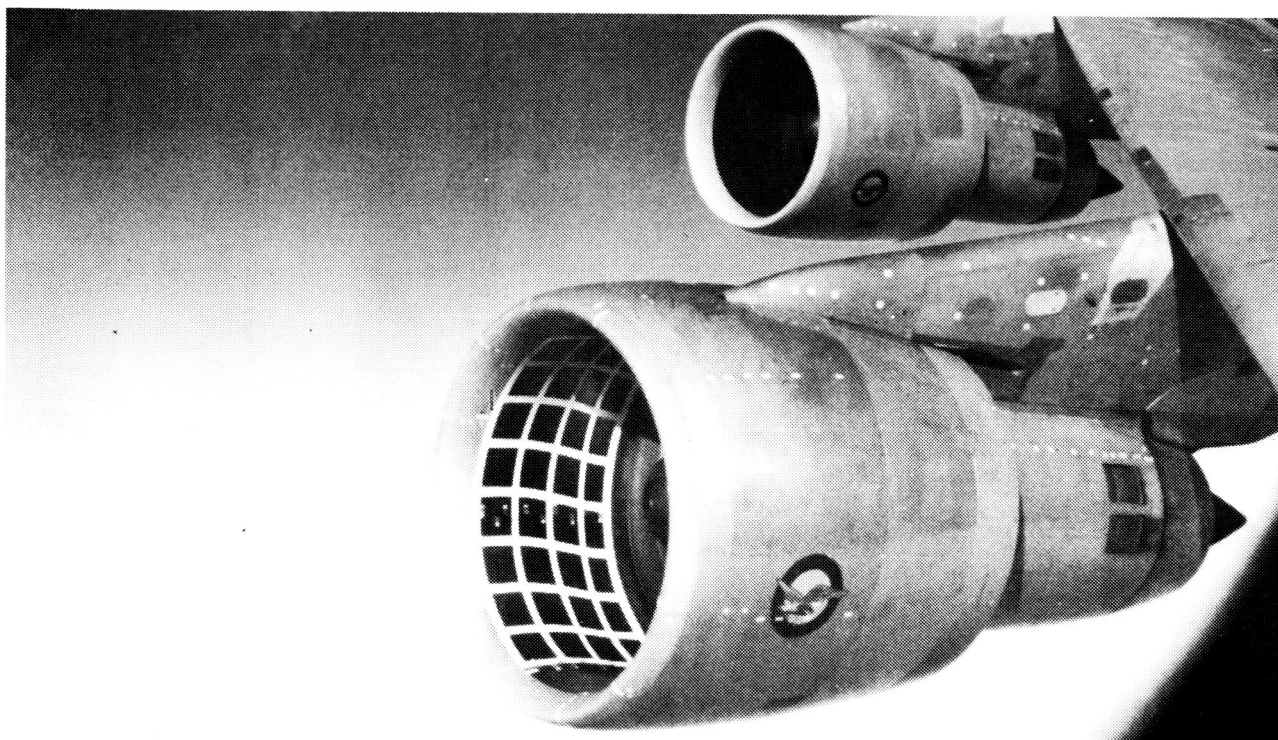
Figure 5. View of Pressure Ports

Figure 6. Pressure Transducer
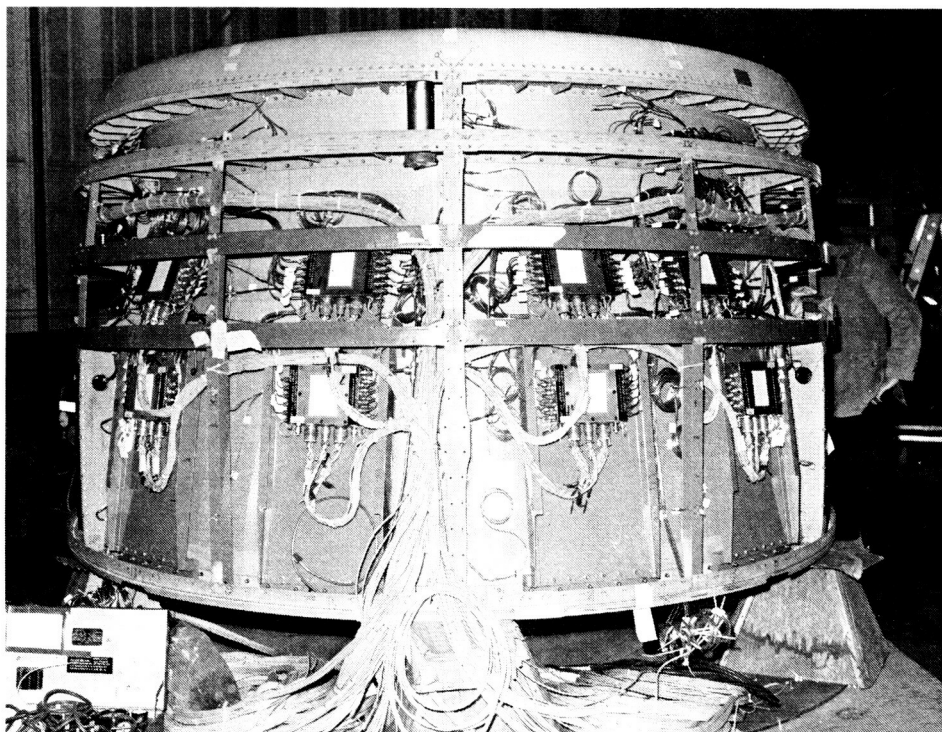
Figure 7. Pressure Transducer Installation
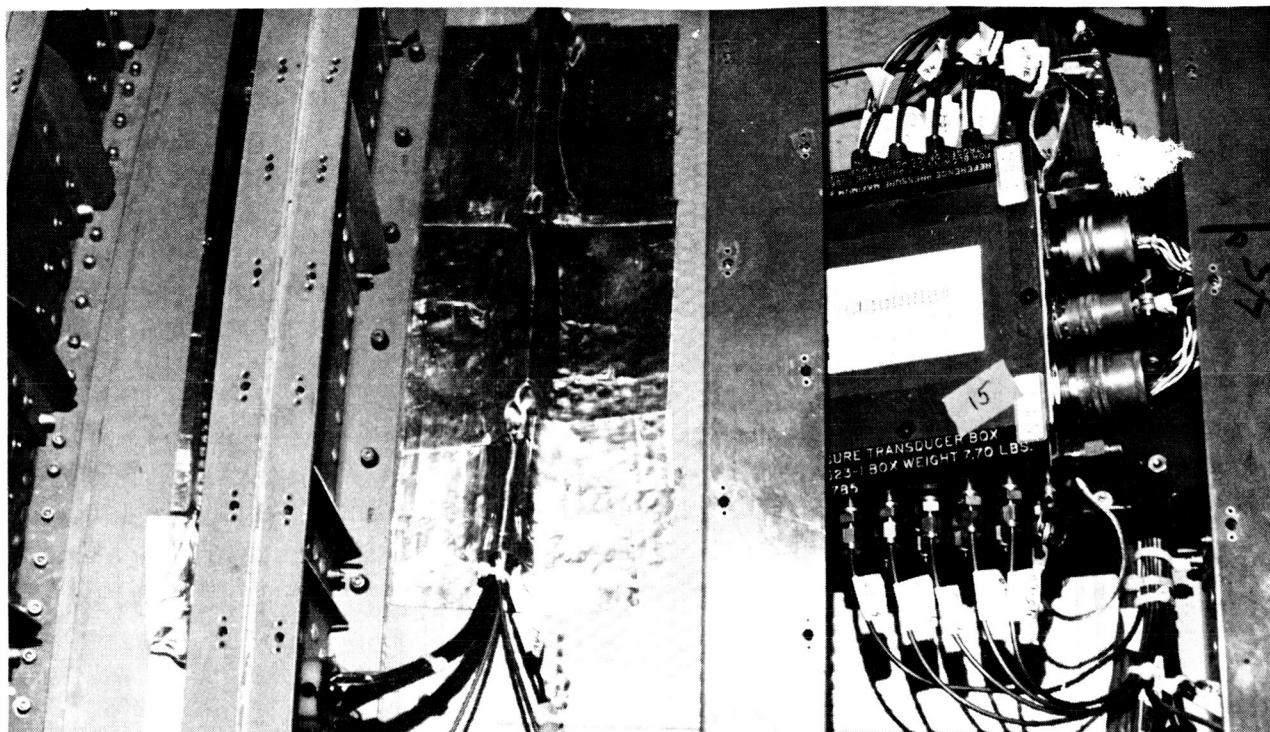
Figure 8. Pressure Transducer Box

Pressure measurements were obtained on the fan cowl doors of engine 3 (fig. 9). The arrangement was two rows of pressure taps, one on each side of both cowl doors, 30 deg from the top. Each pressure tap was connected to its individual transducer by copper tubing except at the hinges of the fan cowl doors, where a small section of copper tubing was replaced by a piece of flexible clear polymer. This flexible section enabled the doors to function throughout the test program.

The pressure instrumentation on engine 4 was designed to substantiate a finding of the feasibility study (ref. 4) that suggested engine deterioration was independent of position. Therefore, engine 4 inlet was instrumented with three rows of 15 pressure taps each spaced 120 deg apart (fig. 10) for a total of 45 measurements. These measurements were sufficient to indicate relative load levels between inboard and outboard inlets.

Inertial Loads Instrumentation—Instrumentation for inertial loads consisted of accelerometers and rate gyros located on the engine and pylon (fig. 11) and the aircraft center of gravity. Linear accelerations were measured by Q-FLEX accelerometers (fig. 12). These instruments were used on both test engines and at their wing and pylon interface. For angular velocities, two axes of a three-axis Northrop rate gyro mounted on the two test engines (fig. 13) were used.

Location of accelerometers and rate gyros is referenced by clock position, looking aft. Accelerometers were placed on the engines so that lateral accelerations were measured in the lateral direction at NAC STA 46 at 3 o'clock and at NAC STA 100 at 6 o'clock. Vertical accelerations were measured at NAC STA 46 at 6 o'clock, NAC STA 100 at 3 o'clock, and NAC STA 100 at 9 o'clock, and longitudinal acceleration was at NAC STA 100 at 6 o'clock. Rate gyros placed at NAC STA 100 at 3 o'clock were used to measure pitch and yaw rate. The six accelerometers on each engine permitted calculation of the linear and angular accelerations at the engine centers of gravity.

16
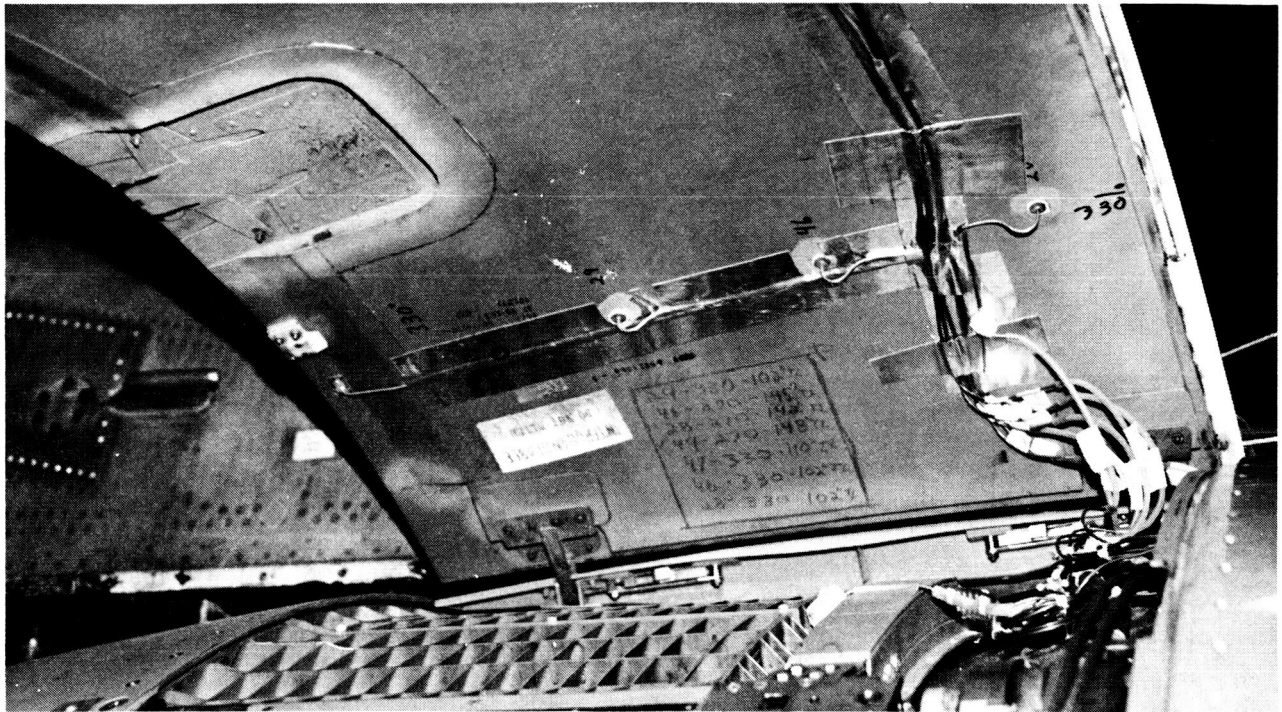
Figure 9. Cowl Door Pressure Taps

45 PORTS

FAN FACE →

● Clockwise from front
  ● 15 each at 60, 180, and 300 deg
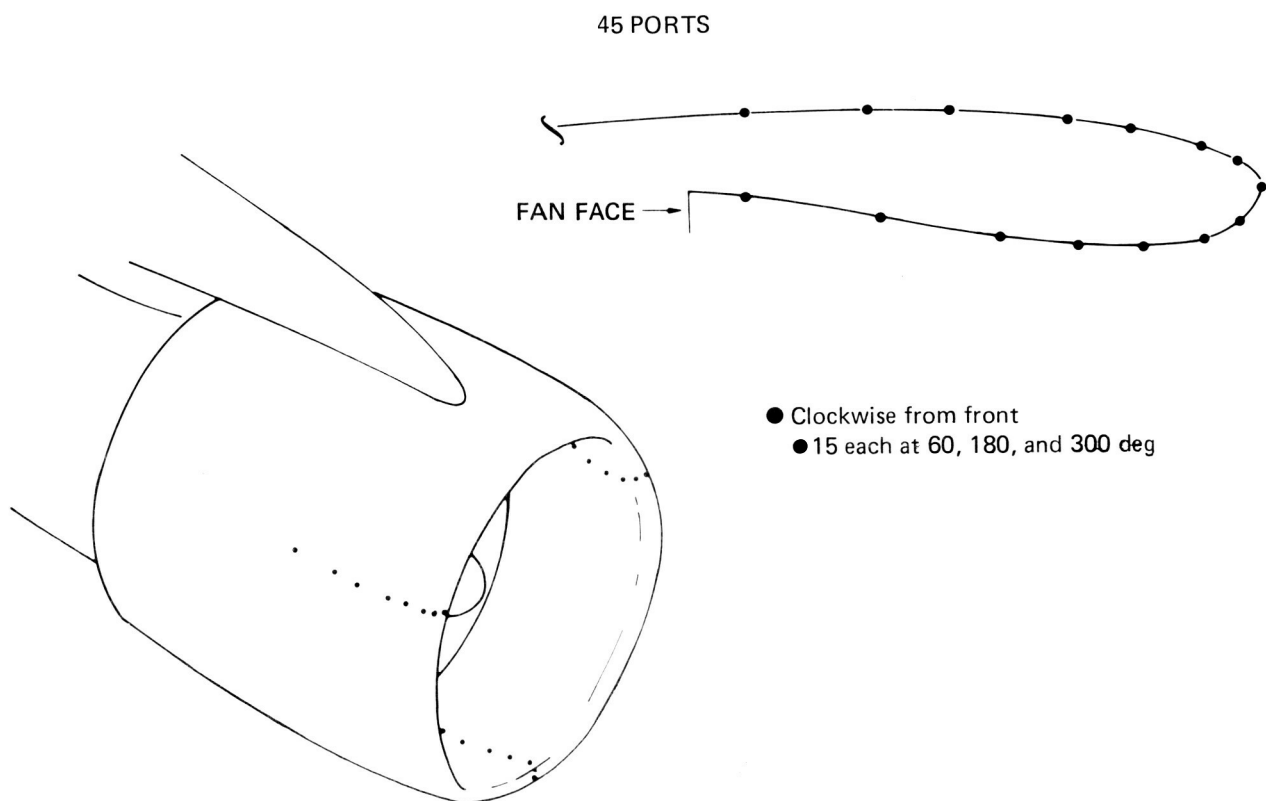
Figure 10. Outboard Engine Pressure Taps

17

● Inboard and outboard engines

SIX NEAR
STRUT ATTACH
POINTS

FRONT
SPAR

FOUR NEAR
FAN FACE

TWO NEAR
INLET TIP
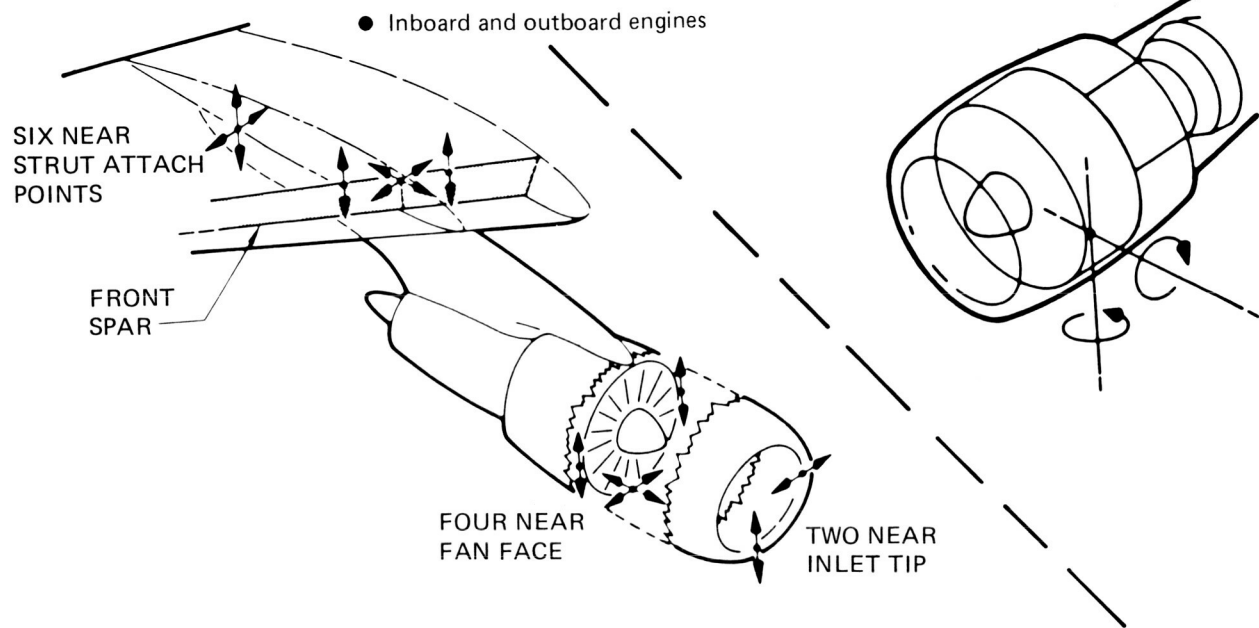
Figure 11. Inertial Data Sensors
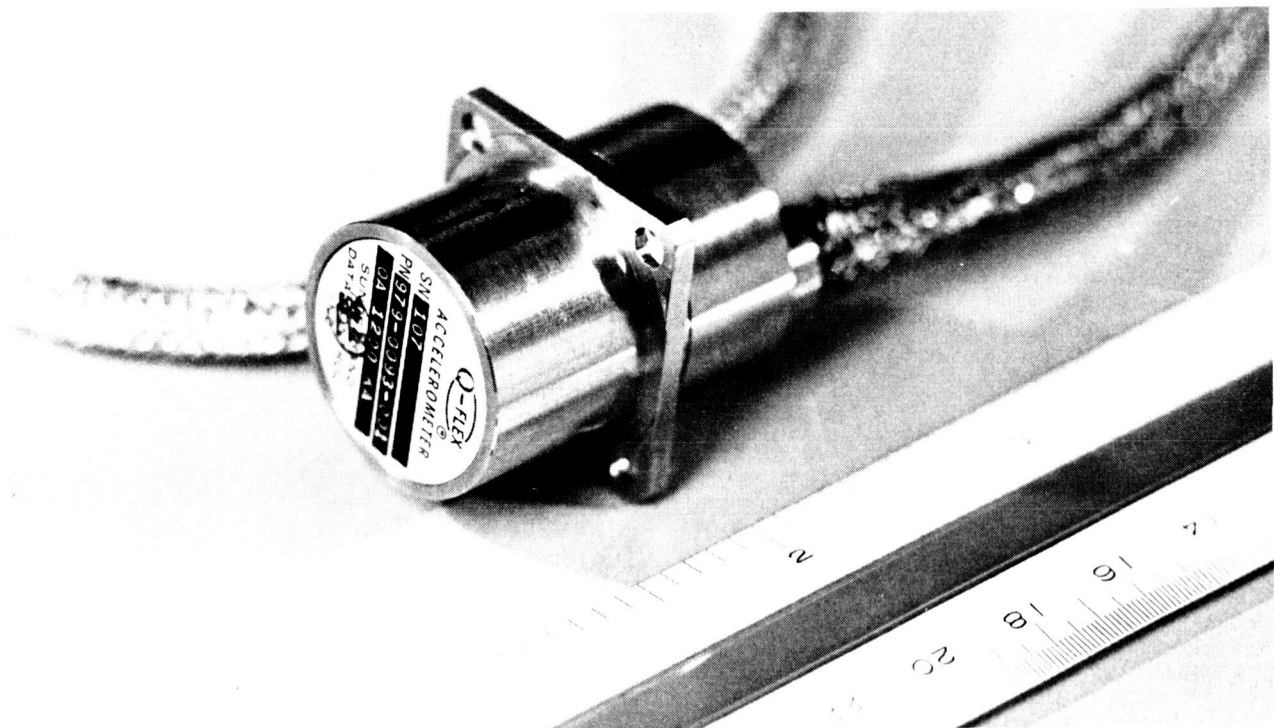
Figure 12. Q-FLEX Accelerometer

18
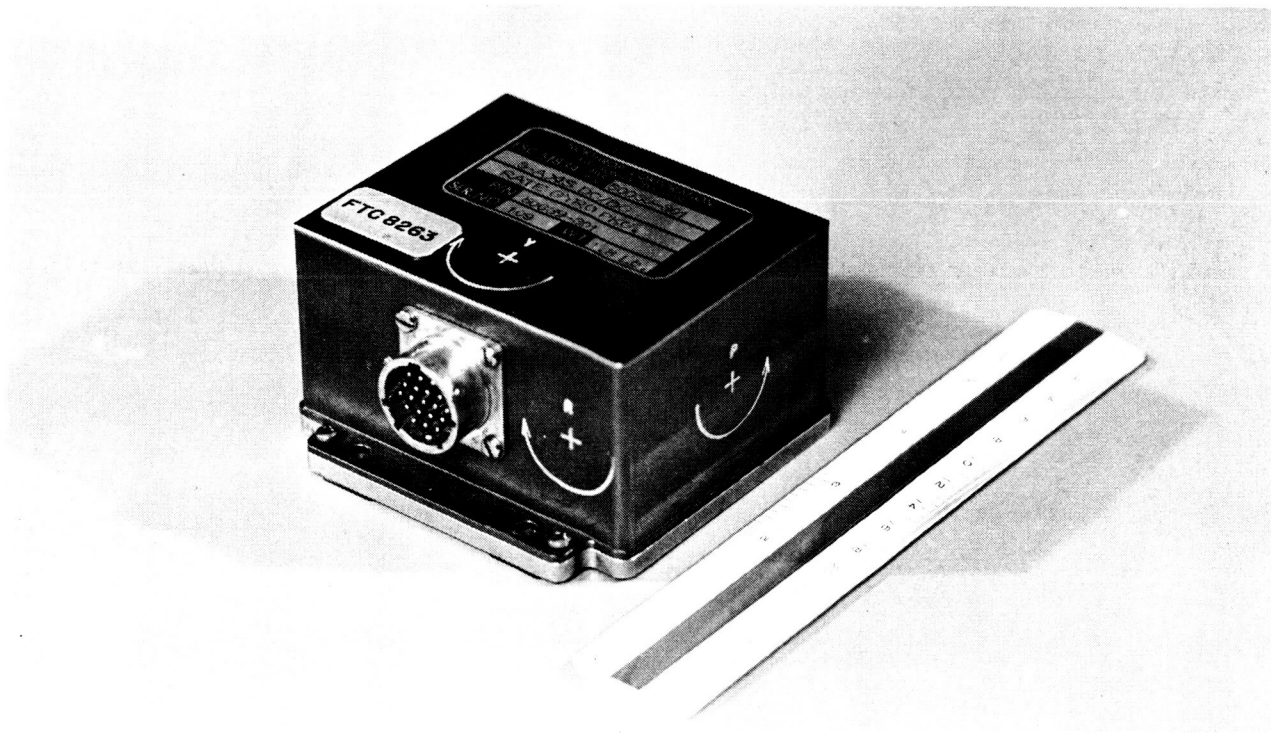
Figure 13. Rate Gyro

Accelerations were measured at the pylon/wing interfaces. The lateral accelerations were measured at the wing front spar and the rear thrust link attach point (fig. 14). The vertical accelerations were measured inboard and outboard of the front spar attach point and on the rear thrust link attach point. In the longitudinal direction, accelerations were measured only at the front spar. Each interface had a total of six linear accelerometers.

Basic airplane information was recorded, including pitch, yaw, and roll angles, along with side-slip and angle of attack. Angular accelerations about all three axes were measured near the aircraft center of gravity.

Clearance Measurement System—Engine clearance change measurements were made by P&WA simultaneously with flight load application. Measurements were made on the fan and first-stage high-pressure turbine on the inboard engine and the fan stage of the outboard engine by a laser proximity system for each stage. Each clearance monitoring system consisted of: (1) the laser assembly (four lasers per box), (2) the input fiber optic assembly, (3) video camera assembly, (4) laser probe assembly (four probes per stage), (5) video monitor, and (6) video tape recorder (fig. 15). The installation is described in detail in reference 5.

In accordance with the interface agreement between the two companies, P&WA provided all clearance monitoring system components and made the necessary engine preparations. Operation and maintenance of the system during testing were also the responsibility of P&WA. P&WA provided to BCAC the equipment necessary for installation in the airplane during the layup period prior to testing.

Engine Performance—Engine performance data were required for the P&WA effort to correlate measured engine clearance changes or closures with performance losses. Primary emphasis was on engine 3, which had complete instrumentation. Minimum

19
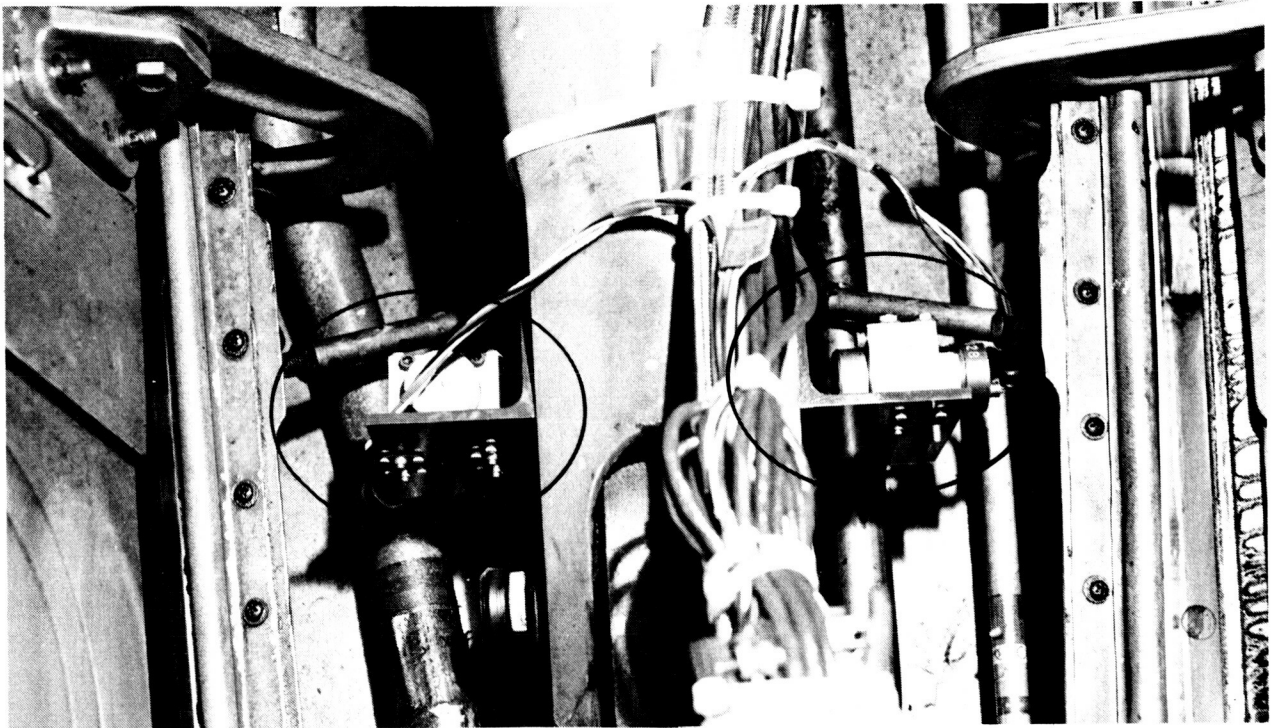
Figure 14. Accelerometer Installation (Thrust Link)
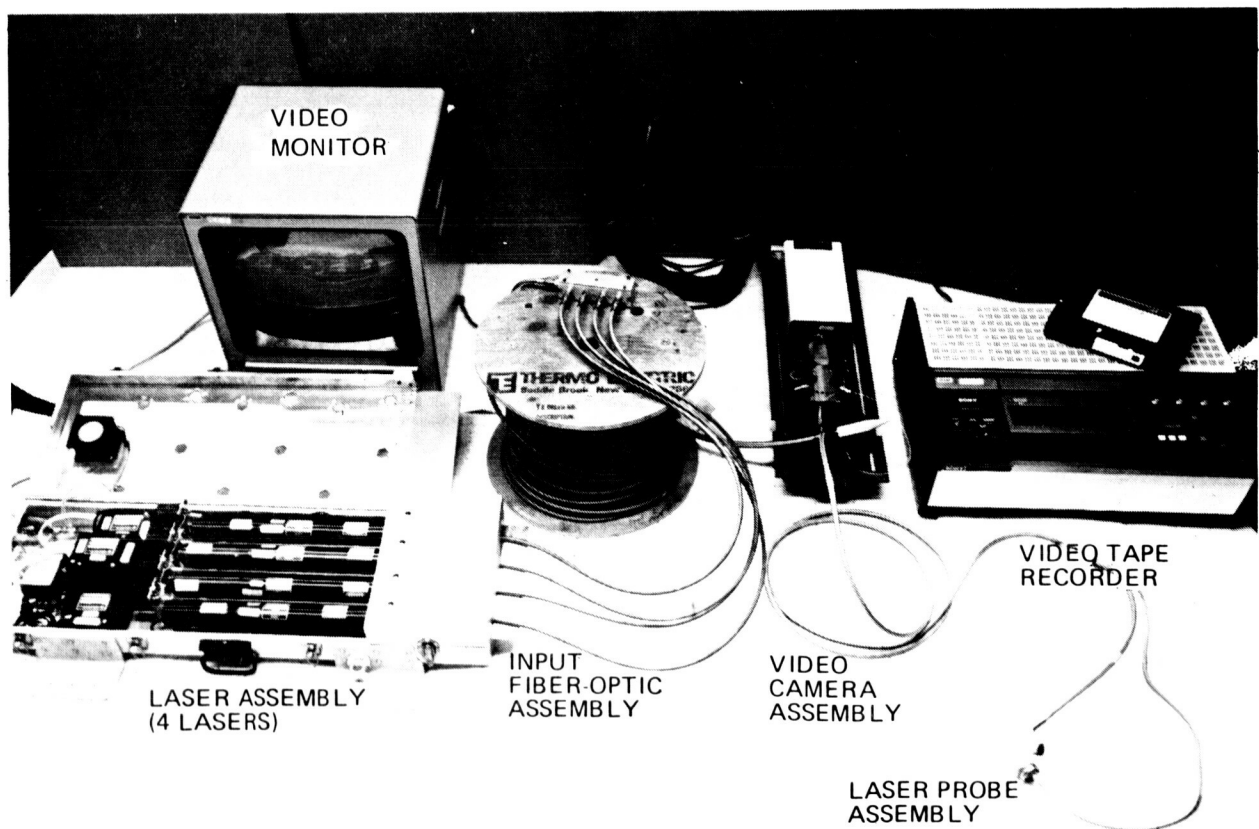
Figure 15. Blade-Tip Clearance Monitoring System

instrumentation to define engine speed and engine airflow and power level was provided for engine 4. Instrumentation for engine 3 was typical of that used for a performance engine test program and was compatible with that used during the pre- and postprogram base engine calibrations at the P&WA Middletown test facility. To better correlate data, the Boeing-owned flight high- and low-rotor speed tachometers (N2 and N1, respectively) and the fuel flow meter were calibrated by P&WA and were used during the pre- and postcalibration at P&WA. The tachometers and flow meter were used on this engine throughout the entire NAIL program.

4.1.2.2 Installed Propulsion System Aerodynamics (IPSA)

In addition to the inlet and fan cowl pressure instrumentation already provided under the flight loads portion of the program, IPSA required pressure measurements on the inboard and outboard pylons, core cowls, and wings. Figure 16 shows the location of external tubing strips used for pressure measurements on the wing upper surface. Three strips were used for each engine; one on the centerline and one on either side. On the lower surface, two strips were used for each engine, located directly below the upper surface's outer strips. Pressure ports on the pylon and core cowl were plumbed internally, and port location marks are visible in figure 5. Because IPSA pressure measurements were required only under steady conditions, it was possible to record the readings using 24-port Scanivalves connected to a Gould Statham differential pressure transducer. (A more detailed description of IPSA instrumentation is given in ref. 5.)
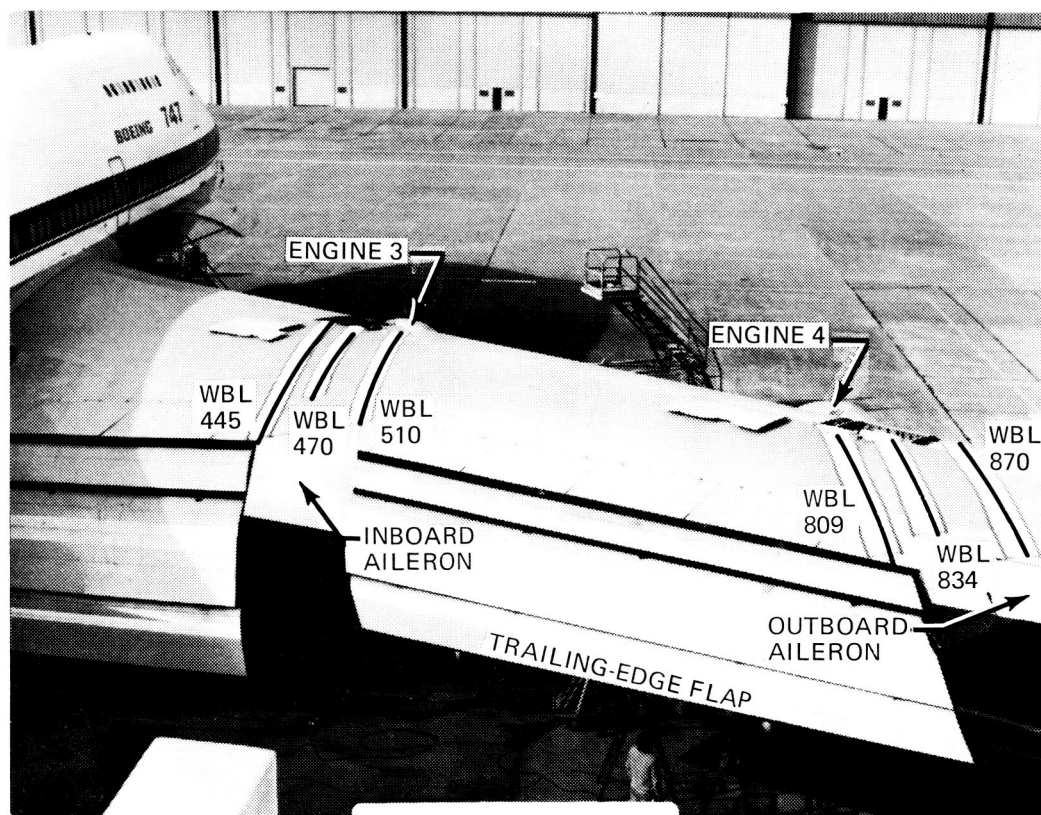
Figure 16. IPSA Wing Pressure Measurement Locations

4.1.3 Test Conditions and Procedures

4.1.3.1 Flight Loads

Testing for performance degradation was accomplished in several distinct stages to measure engine clearance changes resulting from various flight maneuvers. Once the installation and fabrication on the test bed aircraft were completed, an engine ground calibration was performed prior to the functional check flight. This calibration enabled comparison with the test stand calibrations by P&WA and provided a data base line for the flight test program.

It was suspected that the first 0.8% loss in performance due to engine clearance changes occurred during the production acceptance test flight (fig. 17). Therefore, this test profile was chosen as the basis of the first test flight and was followed by a second ground calibration. Subsequent flights contained high-g turns and variations in takeoff gross weight. Under the test plan, each series of tests required a ground calibration after the particular series. Using these calibrations, performance deterioration was determined for each series of tests. The final ground calibration was performed after completing all flight testing. In all, five ground calibrations were conducted during the NAIL flight test program.

- Flight conditions 101 to 115 are further specified in Table 1.
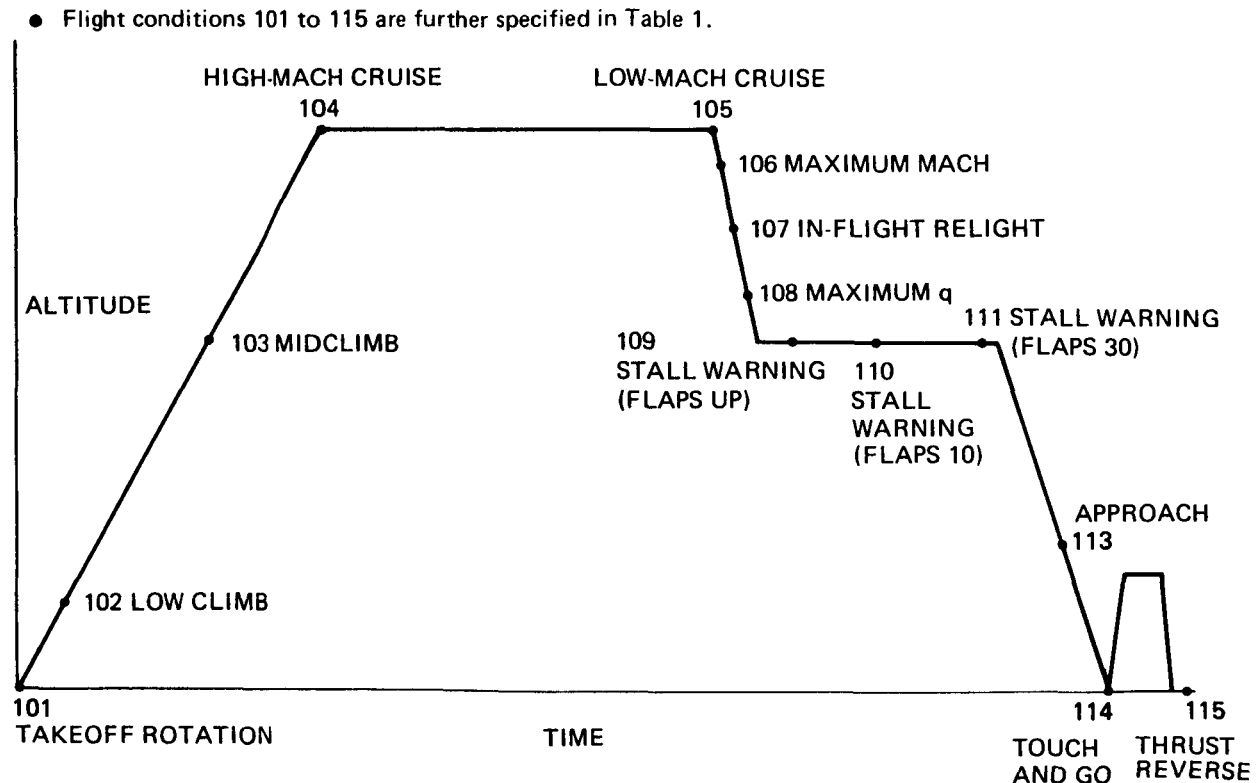
Figure 17. Acceptance Flight Profile

The test conditions actually flown (table 1) resulted from compromise and various flight restrictions. Originally NAIL was to be a standalone flight program. However, the flight test was conducted concurrently with the 767/JT9D-7R4 test program, which imposed certain flight restrictions on RA001. The most significant restrictions were (1) to remain within the 767 design cruise speed and Mach number (V_C and M_C) limits of 667 km/h CAS (360 kcas) and M = 0.86 until the completion of all JT9D-7R4 test conditions and (2) to limit nacelle loads to 80% of the design limit. Upon completion of the JT9D-7R4 program, the 767 design envelope V_D and M_D limits of 778 km/h CAS (420 kcas) and M = 0.91 were applied to the NAIL program.

Because of the absence of inlet anti-ice provisions on the instrumented engines and the need to prevent accumulation and subsequent freezing of water in the pressure tap tubing, no flights were made in visible moisture.

Because a functional check flight and a ferry flight to the remote test site were required prior to any NAIL data collection effort, it was necessary to restrict the level of power to prevent performance losses in the analytically built engine 3. Therefore, all flights prior to the first data flight were limited to an engine pressure ratio (EPR) of 1.18 with no bleeds during takeoff and maintained a locked throttle climb to 3048m (10 000 ft) at which time normal operation resumed.

As a result of the concurrent testing programs, data were taken over approximately 33 hours of flight time instead of over the initially planned 15-hour maximum. The increased flight time resulted in a substantially larger quantity of data to survey and select from

Table 1. Test Conditions Flown

Test condition	Test no.	Event time	Pressure altitude, m (ft)	Mach no.
101 277.6t (612 000 lb) GWTO (flaps 20)	273-7	6:41:44	778.2 (2 553)	0.250
101 244.0t (538 000 lb) GWTO (flaps 10)	273-10	9:44:10	812.9 (2 667)	0.239
101 293.5t (647 000 lb) GWTO (flaps 10)	273-11	10:13:52	802.8 (2 634)	0.254
118 353.8t (780 000 lb) GW simulated TO (flaps 10)	273-15	8:13:18	1 111.3 (3 646)	0.296
102 Low climb	273-10	9:46:00	1 786.4 (5 861)	0.367
103 Mid climb	273-7	7:28:44	5 238.6 (17 187)	0.599
104 High M cruise	273-7	7:49:26	10 814.6 (35 481)	0.859
105 Low M cruise	273-7	7:56:40	10 824.1 (35 512)	0.772
106 Max M	273-15	12:09:27	11 270.9 (36 978)	0.906
107 Inflight relight	273-7	8:12:53	8 491.4 (27 859)	0.721
108 Maximum q	273-15	11:39:00	7 471.6 (24 513)	0.836
109 Stall warning (flaps up)	273-7	8:18:58	5 170.7 (16 964)	0.391
110 Stall warning (flaps 10)	273-7	8:22:26	4 949.7 (16 239)	0.347
111 Stall warning (flaps 30)	273-7	8:24:52	5 196.5 (17 049)	0.270
112 Idle descent	273-7	8:28:56	2 575.6 (8 450)	0.439
113 Approach	273-7	8:34:27	1 829.7 (6 003)	0.265
114 Touch and go	273-7	8:40:36	780.6 (2 561)	0.263
115 Thrust reverse	273-7	8:46:00	780.6 (2 561)	0.179
116 2.0g left turn (flaps up)	273-10	13:33:58	2 559.4 (8 397)	0.487
117 1.6g left turn (flaps 30)	273-10	13:41:07	2 500.0 (8 202)	0.260
120 2.0g right turn (flaps up)	273-15	11:04:03	2 511.5 (8 240)	0.476
121 1.6g right turn (flaps 30)	273-15	11:07:25	2 523.1 (8 278)	0.266
123 Airplane stall	273-10	13:26:17	2 743.2 (9 000)	0.207
124 High gross weight landing	273-15	8:20:49	— —	—

23

and provided additional conditions for analysis.

4.1.3.2 Installed Propulsion System Aerodynamics (IPSA)

Four test conditions were flown in the IPSA portion of the project. Three were in level flight at Mach 0.77, 0.80, and 0.86. The fourth was a shallow dive at Mach 0.91. All were flown at representative cruise altitudes and lift coefficients. A detailed description of the test procedures is given in reference 5, section 4.1.3.2.

4.1.4 Test Data Format

The data collected during the NAIL program required extensive use of the airborne data analysis and monitor system (ADAMS) (fig. 18). Of particular concern was the ability to assess real-time data quality for flight decisions, because 1023 channels of measurements were being made during the combined test program and no ground-based analysis system was available at the remote site. It was necessary to send the flight tape to Seattle shortly after completion of each day's testing. This requirement did not allow rerunning the tape on the ADAMS. Therefore, essentially all decisions were based on real-time displays of data on the ADAMS during flight.
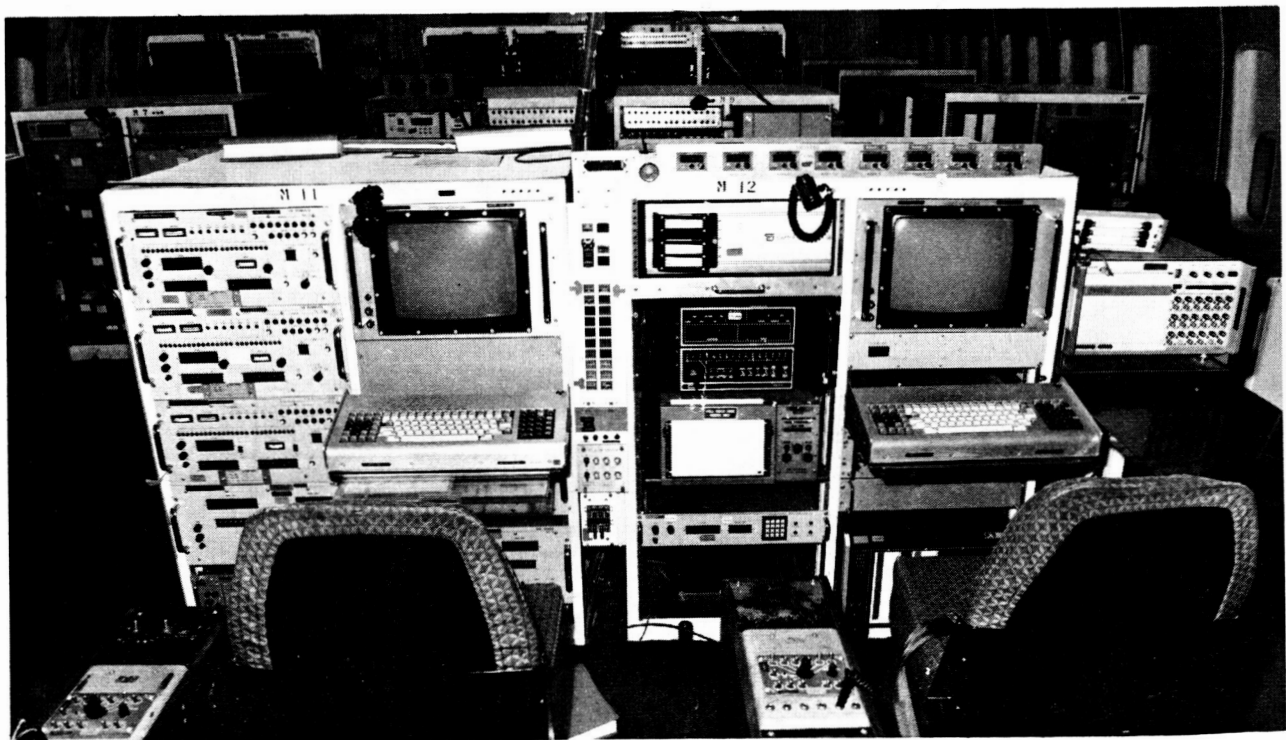
Figure 18. Airborne Data Analysis and Monitoring System (ADAMS)

A single ADAMS could not handle the volume of data required by the JT9D-7R4 and NAIL programs. The expanded data handling capabilities of the analysis groups doubled that of the basic system by using a second ADAMS on the RA001. The quantity of data collected during the program required system modification in order to minimize testing and preflight delays. These modifications to the onboard flight test system (fig. 19) provided adequate remote-base support to the flight test program. Several hardware and software changes to the basic ADAMS were implemented to accomplish this support.

Figure 19. Test Airplane Interior View

Two other significant hardware changes were made to the basic ADAMS. First, a fixed head disk for program and measurement information storage was used. The fixed head disk eliminated loading information from tapes each time the system was brought online. This improvement was vital because activating the system required 1 to 2 min rather than 15 min as projected, based on the number of measurements required. A 15-min delay was unacceptable in terms of cost, if the system should malfunction once airborne. Further, rapid selection of preselected data sources was also a requirement in view of the quantity of data being measured and the concurrent test program to permit the test engineers to track their respective data. Second, a data measurement selector was incorporated into the ADAMS. This was necessary because measurements for approximately 1023 parameters were obtained during the flight test. The data measurement selector sent data preselected for output to the digital-to-analog converter.

The original ADAMS software could not support the NAIL program during remote base operation. An onboard pressure coefficient program was lacking, and thus development of an interim program that satisfied the needs of analysis was necessary. The program was developed to use the Brush recorder as a quasigraphics system and to use the line printer for summary outputs. The program could calculate pressure coefficients for up to 16 measurement groups with a maximum of 20 pressure ports each. The output of the program was displayed on the Brush recorder while a summary table of port differential pressures and pressure coefficient values was printed on the line printer. This information was output either continuously or upon keyboard command for a predetermined time interval. The program provided real-time information for determining data quality and for making decisions on subsequent test conditions.

Final data were supplied as tables, computer-generated graphs, and data files on magnetic tapes. Table 2 is an example of pressure coefficient data. Table 3 is an example of engine performance data, including airflow.

25

Table 2. Example of Tabulated Pressure Coefficient Data

AIRPLANE MODEL 747-100
AIRPLANE NUMBER RA001

TEST 273-07 PRESSURE COEFFICIENT

COORDINATION TIME HR-MIN-SEC	CE DEG	ALPHA DEG	Q PSI	PRESS-INLET E3 PT01 240R PS 3211	PT01 CP	PRESS-INLET E3 PT02 240R PS 3212	PT02 CP	PRESS-INLET E3 PT03 240R PS 3213	PT03 CP	PRESS-INLET E3 PT04 240R PS 3214	PT04 CP	PRESS-INLET E3 PT05 240R PS 3215	PT05 CP	PRESS-INLET E3 PT06 240R PS 3216	PT06 CP
			IEC	IEC	IEC	IEC	IEC	IEC	IEC	IEC	IEC	IEC	IEC	IEC	IEC
8-33-20.014	DNA	DNA	0.495	11.296	-1.040	11.152	-1.220	10.994	-1.506	10.871	-1.794	10.620	-2.256	10.487	-2.555
8-33-20.064	DNA	DNA	0.495	11.225	-1.126	11.136	-1.187	10.994	-1.506	10.852	-1.794	10.603	-2.227	10.475	-2.491
8-33-20.114	DNA	DNA	0.495	11.182	-1.098	11.152	-1.188	11.054	-1.364	10.852	-1.717	10.618	-2.262	10.512	-2.504
8-33-20.164	DNA	DNA	0.495	11.197	-1.126	11.152	-1.155	10.994	-1.506	10.890	-1.717	10.620	-2.192	10.493	-2.532
8-33-20.214	DNA	DNA	0.495	11.182	-0.953	11.168	-1.155	11.029	-1.435	10.890	-1.673	10.655	-2.172	10.487	-2.532
8-33-20.264	DNA	DNA	0.495	11.254	-1.040	11.184	-1.155	10.994	-1.507	10.909	-1.795	10.655	-2.223	10.487	-2.497
8-33-20.314	DNA	DNA	0.495	11.211	-0.858	11.168	-1.058	11.029	-1.436	10.852	-1.756	10.638	-2.263	10.590	-2.553
8-33-20.364	DNA	DNA	0.495	11.210	-1.012	11.215	-1.155	11.082	-1.329	10.871	-1.755	10.621	-2.263	10.437	-2.507
8-33-20.414	DNA	DNA	0.495	11.118	-0.897	11.152	-1.155	11.030	-1.436	10.871	-1.756	10.603	-2.265	10.475	-2.507
8-33-20.464	DNA	DNA	0.495	11.296	-0.782	11.168	-1.123	11.030	-1.436	10.871	-1.717	10.621	-2.252	10.500	-2.557
8-33-20.514	DNA	DNA	0.495	11.353	-0.954	11.184	-1.123	10.977	-1.542	10.891	-1.755	10.621	-2.252	10.500	-2.557
8-33-20.564	DNA	DNA	0.495	11.268	-1.040	11.184	-1.091	10.995	-1.507	10.891	-1.833	10.621	-2.263	10.550	-2.554
8-33-20.614	DNA	DNA	0.495	11.225	-1.011	11.200	-1.188	10.935	-1.507	10.833	-1.755	10.637	-2.263	10.475	-2.559
8-33-20.664	DNA	DNA	0.495	11.240	-1.040	11.152	-1.318	11.012	-1.471	10.852	-1.795	10.638	-2.254	10.529	-2.494
8-33-20.714	DNA	DNA	0.495	11.226	-1.012	11.038	-1.221	11.030	-1.436	10.852	-1.718	10.621	-2.194	10.513	-2.534
8-33-20.764	DNA	DNA	0.494	11.240	-1.041	11.226	-1.059	11.012	-1.472	10.872	-1.757	10.656	-2.264	10.513	-2.559
8-33-20.814	DNA	DNA	0.494	11.256	-0.984	11.137	-1.221	11.012	-1.472	10.891	-1.583	10.635	-2.229	10.475	-2.556
8-33-20.864	DNA	DNA	0.494	11.212	-1.070	11.217	-1.124	11.030	-1.437	10.891	-1.757	10.621	-2.254	10.463	-2.505
8-33-20.914	DNA	DNA	0.494	11.254	-0.984	11.137	-1.091	11.013	-1.472	10.910	-1.756	10.604	-2.229	10.476	-2.533
8-33-20.964	DNA	DNA	0.494	11.211	-0.840	11.185	-0.962	11.043	-1.401	10.872	-1.718	10.639	-2.264	10.501	-2.511
8-33-21.014	DNA	DNA	0.494	11.325	-1.041	11.201	-1.156	11.013	-1.472	10.853	-1.795	10.604	-2.199	10.493	-2.532
8-33-21.064	DNA	DNA	0.494	11.226	-0.840	11.265	-1.221	11.013	-1.472	10.891	-1.756	10.622	-2.222	10.476	-2.557
8-33-21.114	DNA	DNA	0.494	11.311	-1.041	11.169	-1.188	11.030	-1.437	10.891	-1.833	10.622	-2.262	10.513	-2.451
8-33-21.164	DNA	DNA	0.494	11.254	-0.868	11.137	-1.220	11.043	-1.401	10.853	-1.673	10.659	-2.191	10.511	-2.505
8-33-21.214	DNA	DNA	0.494	11.283	-0.983	11.137	-1.155	11.013	-1.472	10.872	-1.755	10.691	-2.226	10.525	-2.379
8-33-21.264	DNA	DNA	0.494	11.297	-0.926	11.153	-1.187	10.978	-1.543	10.834	-1.677	10.674	-2.191	10.553	-2.455
8-33-21.314	DNA	DNA	0.495	11.240	-0.897	11.153	-1.155	10.950	-1.579	10.949	-1.599	10.672	-2.155	10.553	-2.351
8-33-21.364	DNA	DNA	0.495	11.155	-1.012	11.169	-1.056	10.995	-1.507	10.911	-1.677	10.659	-2.291	10.505	-2.555
8-33-21.414	DNA	DNA	0.495	11.198	-1.184	11.153	-1.122	11.031	-1.577	10.872	-1.871	10.691	-2.472	10.390	-2.406
8-33-21.464	DNA	DNA	0.495	11.269	-1.059	11.218	-1.057	10.960	-1.399	10.911	-1.957	10.674	-2.332	10.414	-2.382
8-33-21.514	DNA	DNA	0.495	11.226	-1.097	11.269	-1.187	11.045	-1.470	10.815	-1.794	10.672	-2.157	10.476	
8-33-21.564	DNA	DNA	0.495	11.283	-0.953	11.218	-1.155	11.013	-1.399	10.753	-1.601	10.587	-2.087	10.551	
8-33-21.614	DNA	DNA	0.495	11.241	-1.039	11.154	-1.123	11.048	-1.364	10.854	-1.601	10.674		10.563	
8-33-21.664	DNA	DNA	0.495	11.284	-0.925	11.186	-1.123	11.056	-1.435	10.950		10.709			
8-33-21.714	DNA	DNA	0.495	11.340	-1.011	11.186	-1.123	11.031	-1.505	10.950					
8-33-21.764	DNA	DNA	0.495	11.255	-0.925	11.186	-1.123	11.031	-1.471						
8-33-21.814	DNA	DNA	0.495	11.213	-0.810			10.976	-1.436						
8-33-21.864	DNA	DNA	0.495		-0.983			11.014							
8-33-21.914	DNA	DNA	0.495		-1.069			11.031							
8-33-21.964	DNA	DNA	0.495												

Table 3. Sample Tabulation of Engine Performance Data

AIRPLANE MODEL 747-100   TEST 273-15   JT9 ENG PERF SUMMARY   REQUEST NO 1316.0101
AIRPLANE NUMBER RA001   DATE 10/31/80 TIME 0515

AIRPLANE DATA

HP FEET	M	V KTS	DELTAM DEG C	TAM DEG C	TTI DEG C	DELAMB	PSI IN HG	PTI IN HG	DELTI	THEA67	THET67	THET91	THETS7
24076.	0.601	364.8	2.5	-30.2	-12.7	0.3863	11.56	14.75	0.4930	0.8920	0.9346	NDA	NDA

GAS GENERATOR SUMMARY

ENG STS	FN RFN LBS	SFC RSFC	N1 RN1 RPM	N2 RN2 RPM	T6 RT6 C/K	T7 RT7 C/K	WF RWF LB/HR	WAT RWAT LB/SC	P25PT1 PT7PT1	PS4 PS4PT7	SBV BPR POS/	SVA SGF DEG/	PLA DEG
1 NDA	NDA / NDA	IDU / IDU	NDA / NDA	NDA / NDA	NDA / NDA	NDA / NDA	IDU / IDU	NDA / NDA	NDA / NDA	NDA / NDA	NDA / NDA	NDA 0.8213	NDA
2 NDA	NDA / NDA	IDU / IDU	NDA / NDA	NDA / NDA	NDA / NDA	NDA / NDA	IDU / IDU	NDA / NDA	NDA / NDA	NDA / NDA	NDA / NDA	NDA 0.8213	NDA
3 NDA	7212. / 18670.	0.6979 / 0.7824	2780. / 2924.	6644. / 6988.	620. / 979.	400. / 749.	5039. / 10938.	725. / 1398.	1.335 / 1.092	205.527 / 12.763	1.0 / 6.37	0.4 0.8213	72.1
4 NDA	NDA / NDA	IDU / IDU	NDA / NDA	NDA / NDA	NDA / NDA	NDA / NDA	IDU / IDU	NDA / NDA	NDA / NDA	NDA / NDA	NDA / NDA	NDA 0.8213	NDA

THRUST CALCULATION DETAIL SUMMARY

ENG	FGF RFGF LBS	FGP RFGP LBS	FRAM RFRAM LBS	WIF WIP LB/SC	P25PAM PRFPA	P77PAM PRPPA	PTMRP PTBRF	PTMBF	CGF CDF	CGP CDP	AFAN APRI FT2	RT2.5 WBA K/PPS	WFFN WH2O LB/SC	GPRI RPRI
1	NDA / NDA	NDA / NDA	NDA / NDA	NDA / NDA	NDA / NDA	NDA / NDA	NDA / NDA	NDA	NDA / NDA	NDA / NDA	20.119 / 6.641	NDA / NDA	NDA / 7.220	NDA / 0.0
2	NDA / NDA	NDA / NDA	NDA / NDA	NDA / NDA	NDA / NDA	NDA / NDA	NDA / NDA	NDA	NDA / NDA	NDA / NDA	0.0 / 0.0	NDA / NDA	NDA / 7.220	NDA / 0.0
3	17697. / 45812.	3384. / 8760.	13869. / 35902.	646. / 102.	1.7034 / 1.6954	1.3932 / 1.3709	1.0162 / 1.0047	1.0000	0.9441 / 0.9698	0.9473 / 0.9723	20.119 / 6.641	318. / 0.0	1.306 / 7.220	1.359 / 0.0
4	NDA / NDA	NDA / NDA	NDA / NDA	NDA / NDA	NDA / NDA	NDA / NDA	NDA / NDA	NDA	NDA / NDA	NDA / NDA	20.102 / 6.644	NDA / NDA	NDA / 7.220	NDA / 0.0

ALL VALUES PRINTED ARE CONDITION AVERAGES

PROGRAM LIBRARY 08/11/80 PR07   CONDITION NO 4.08.015.007
DOCUMENT NO D6-22119-1
PAGE NO

4.2 TEST RESULTS

4.2.1 Aerodynamic and Inertial Loads

4.2.1.1 Aerodynamic Loads

Pressures were measured at 252 ports in 12 rows nominally 30 deg apart on the inlet and fan cowl of engine 3. The actual spacing varied slightly for some ports because of installation and arrangement requirements. Fourteen ports were found to have defective or doubtful transducers, and the indicated pressures of those ports were not used. Pressure data are presented graphically and in tabular form in Appendix A of reference 3, along with port location details.

To compute resultant airloads from the pressure data, a previously developed computer program was used. It approximated the inlet and cowl geometry as a series of conical frustums and adjusted for the tilt of the inlet axis with respect to the nacelle centerline by insertion of wedge-shaped surfaces. This procedure was checked by comparison to a method based on a complete three-dimensional geometry definition. Resultant forces differed by less than 3%, and resultant yawing and pitching moments at the engine face differed by less than 1%. (Rolling moments differed by 3.5% but are not significant loads.)

Figure 20 shows the coordinate system and sign conventions used. Note that the coordinate axis labels are not those commonly used for airplane body axes. In this report, the z axis coincides with the engine shaft axis and is positive aft. The x (vertical) axis is defined by the intersection of the center plane of the nacelle strut and the plane of the engine front face* and is positive upward. The axis is normal to x and z and is positive inboard. (This is a right-handed system for engine positions 3 and 4. Nose up pitching moments are negative.)
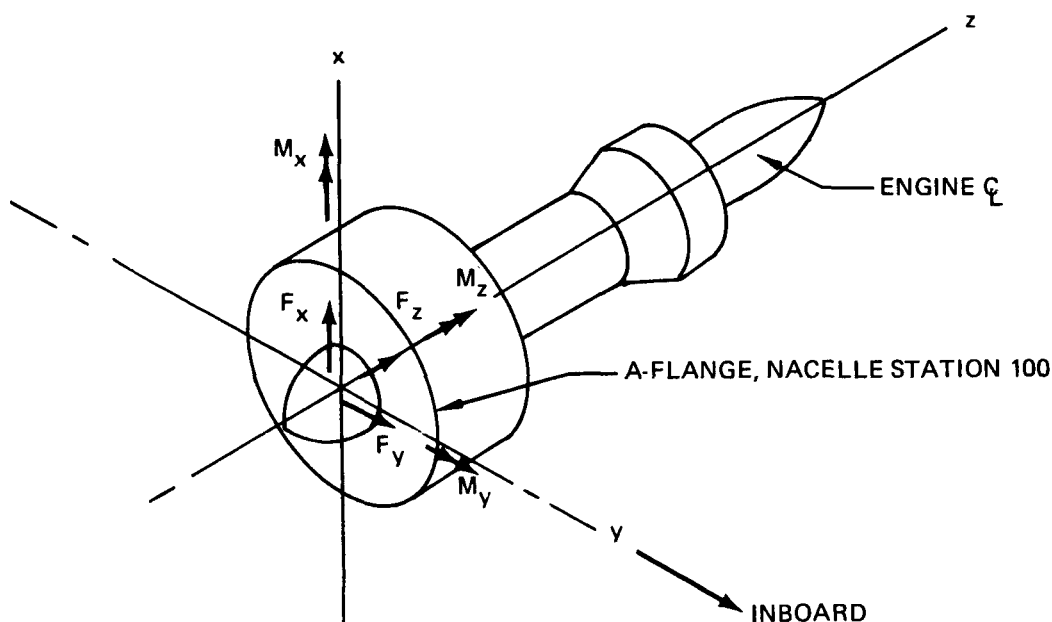

Figure 20. Sign Convention for Steady-State Loads, Engine 3

---

*The inlet is attached and inlet loads are transmitted to the engine bolts through the A-flange at this face.

28

The effect of measurement error on the accuracy of the loads has been estimated on the basis of error calibrations of the Endevco 8510 pressure transducers. The highest root mean square (rms) error of these transducers is 226 Pa (0.0328 lb/in^2) at the extreme range encountered.

This implies the following upper bounds for the rms error of the resultants:

F_x and F_y	921 N (207 lb)
F_z	681 N (153 lb)
M_x and M_y	1226 N-m (10 850 in-lb)
M_z	802 N-m (7100 in-lb)

The relative error for the largest M_y is about $\pm 2.4\%$, and about $\pm 5\%$ for M_x.

Table 4 gives resultant loads along with key airplane and engine parameters for 23 flight conditions.

Other cases given special attention were the turns at constant altitude to achieve a specified load factor. Engine clearance changes during these maneuvers were due to a combination of aerodynamic loads, g-loads, and gyroscopic loads. Condition 116, nominally a 2g turn to the left, was run during test 273-10 and achieved a load factor of 1.99 at IRIG 13:33:58. The A-flange moment was 29 850 N-m (264 200 in-lb). The indicated pitch rate was 4.29 deg/s and the yaw rate was about 2.9 deg/s on both engines. A 2g turn to the right was performed during test 273-15 (condition 120) at IRIG 11:04:03. The moment was 27 100 N-m (239 500 in-lb), pitch rate was 5.5 deg/s, and yaw rate was 2.8 deg/s. Turns of 1.6g at flaps 30 deg were performed to the right and to the left. The left turn occurred during test 273-10, IRIG 13:41:07 (condition 117) with a moment of 32 150 N-m (284 600 in-lb), pitch rate of 6.5 deg/s, and yaw rate of 3.7 deg/s. The right turn occurred during test 273-15 (condition 121) at IRIG 11:07:25 with a moment of 31 900 N-m (282 000 in-lb), pitch rate of 7 deg/s, and yaw rate of 4.7 deg/s. Finally, an airplane stall occurred during test 273-10. The moment peaked at 41 500 N-m (367 000 in-lb) at IRIG 13:26:16. This relatively high load level resulted from a very high angle of attack.

So far all loads presented in this section pertain to engine 3. Preliminary review of the test data indicated that the pressures on engine 4 were very close to the pressures of engine 3, implying that the loads were about equal. Comparison of the aerodynamic loads determined in the NAIL program with the loads predicted as part of the analytical studies of the impact of flight loads on engine performance (ref. 3), indicates that:

- The most critical operating loads were higher than predicted because of higher angles of attack than had been expected.

- The cosine law for the circumferential pressure distribution is only a rough approximation of the actual distribution, especially in the critical region near the "highlight" (front edge of inlet lip).

- The minimum pressure is skewed about 20 deg from the vertical near the highlight, but the skew angle approaches 0 deg further into the inlet.

29

Table 4. Engine 3 Resultant Airloads

Condition	Calibrated airspeed km/h	(kcas)	Pressure altitude, m	(ft)	Mach number	Referred airflow, kg/s	(lb/s)	Load factor, g	F_x, N	(lb)	F_y, N	(lb)	M_x, N-m	(in-lb)	M_y, N-m	(in-lb)
101 Takeoff, 277.6t (612 000 lb) GW (flaps 20)	292.4	(157.8)	778.1	(2 553)	0.250	702.6	(1 549)	1.14	26 694	(6 001)	-12 250	(-2 754)	-16 692	(-147 736)	-37 148	(-328 780)
101 Takeoff, 244.0t (538 000 lb) GW (flaps 10)	279.8	(151.0)	812.9	(2 667)	0.239	692.6	(1 527)	1.26	32 012	(7 197)	-12 970	(-2 916)	-17 207	(-152 292)	-45 280	(-400 756)
101 Takeoff, 293.5t (647 000 lb) GW (flaps 10)	296.7	(160.1)	802.8	(2 634)	0.254	691.3	(1 524)	1.17	35 233	(7 921)	-13 842	(-3 112)	-18 002	(-159 325)	-48 018	(-424 987)
118 Simulated takeoff, 353.8t (780 000 lb) GW (flaps 10)	340.2	(183.6)	1 111.3	(3 646)	0.296	713.5	(1 573)	1.20	37 114	(8 344)	-12 263	(-2 757)	-15 145	(-134 045)	-48 602	(-430 154)
102 Low climb	405.5	(218.8)	1 786.4	(5 861)	0.367	698.1	(1 539)		20 777	(4 670)	-4 746	(-1 067)	-5 125	(-45 361)	-23 280	(-206 043)
103 Mid climb	538.2	(290.4)	5 238.6	(17 187)	0.599	735.7	(1 622)		18 166	(4 084)	-2 615	(-588)	-2 910	(-25 756)	-14 224	(-125 891)
104 High M cruise	539.8	(291.3)	10 814.6	(35 481)	0.859	740.7	(1 633)		10 982	(2 469)	-4 551	(-1 023)	-4 103	(-36 317)	-6 716	(-59 441)
105 Low M Cruise	478.7	(258.3)	10 824.1	(35 512)	0.772	727.6	(1 604)		15 470	(3 478)	-5 031	(-1 131)	-4 772	(-42 237)	-11 994	(-106 150)
106 Max M	554.1	(299.0)	11 270.9	(36 978)	0.906	744.8	(1 642)		1 343	(302)	-2 064	(-464)	-1 783	(-15 779)	2 183	(19 317)
107 Inflight relight	529.5	(285.7)	8 491.4	(27 859)	0.721	619.2	(1 365)		14 576	(3 277)	-3 274	(-736)	-2 897	(-25 639)	-9 587	(-84 847)
108 Maximum q	662.5	(357.5)	7 471.6	(24 513)	0.836	733.5	(1 617)		-6 272	(-1 410)	4 377	(984)	3 283	(29 060)	11 119	(98 411)
109 Stall warning (flaps up)	349.1	(188.4)	5 170.7	(16 964)	0.391	721.7	(1 591)		24 184	(5 437)	-6 156	(-1 384)	-7 206	(-63 775)	-27 480	(-243 214)
110 Stall warning (flaps 10)	313.6	(169.2)	4 949.7	(16 239)	0.347	735.3	(1 621)		27 707	(6 229)	-9 528	(-2 142)	-10 962	(-97 024)	-34 435	(-304 770)
111 Stall warning (flaps 30)	239.6	(129.3)	5 196.5	(17 049)	0.270	740.7	(1 633)		17 467	(3 927)	-5 747	(-1 292)	-8 236	(-72 893)	-24 940	(-220 730)
112 Idle descent	462.7	(249.7)	2 575.6	(8 450)	0.439	339.3	(748)		18 370	(4 130)	-5 000	(-1 124)	-3 352	(-29 669)	-10 986	(-97 234)
113 Approach	291.7	(157.4)	1 829.7	(6 003)	0.265	701.7	(1 547)		16 489	(3 707)	-6 276	(-1 411)	-8 091	(-71 607)	-22 807	(-201 854)
114 Touch and go	308.6	(166.5)	780.6	(2 561)	0.265	720.8	(1 589)		19 518	(4 388)	-10 324	(-2 321)	-14 194	(-125 622)	-27 304	(-241 654)
115 Thrust reverse	209.8	(113.2)	780.6	(2 561)	0.179	621.0	(1 369)		196	(44)	-144	(-10)	-1 954	(-17 298)	-4 628	(-40 963)
116 2.0g left turn (flaps up)	514.3	(277.5)	2 559.4	(8 397)	0.487	708.5	(1 562)	1.99	32 079	(7 212)	-15 386	(-3 459)	-15 060	(-133 292)	-29 850	(-264 186)
117 1.6g left turn (flaps 30)	265.0	(143.0)	2 500.0	(8 202)	0.260	698.1	(1 539)	1.61	23 543	(5 293)	-16 333	(-3 672)	-21 605	(-191 221)	-32 151	(-284 557)
120 2.0g right turn (flap up)	504.3	(272.1)	2 511.6	(8 240)	0.476	542.5	(1 196)	2.04	33 956	(7 634)	-7 246	(-1 629)	-5 362	(-47 455)	-27 058	(-239 481)
121 1.6g right turn (flaps 30)	280.4	(151.3)	2 523.1	(8 278)	0.266	650.9	(1 435)	1.60	24 090	(5 416)	-1 597	(-359)	-1 142	(-10 105)	-31 865	(-282 023)
123 Airplane stall	214.4	(115.7)	2 743.2	(9 000)	0.207	703.5	(1 551)		27 00t	(6 072)	-7 175	(-1 613)	-10 076	(-89 181)	-41 446	(-366 818)

4.2.1.2 Inertial Loads

Normal accelerations measured during takeoff and flight did not exceed 1.3g except during the high-g turn maneuvers. No significant turbulence was experienced during the NAIL program. The difference between g-loads measured at the airplane center of gravity and those measured on engines 3 and 4 was within the scatter of the data. In other words, the instruments responded only to steady-state accelerations of the whole airplane, experiencing no significant contributions from wing or nacelle flexible modes.

An exception to the steady-state accelerations occurred during a hard landing in test 273-15. The airplane landed at 313t (690 000 lb) gross weight with 135t (297 000 lb) of fuel and a sink rate of approximately 1.5 m/s (5 ft/s). Vertical acceleration at the airplane center of gravity was 1.53g, with peaks of 2g at engine 4 and 1.7g at engine 3. Another exception occurred during test 273-10 during which a mild gust was encountered at IRIG 12:11:52. Normal accelerations were 1.08g at the airplane center of gravity and 1.3g at the engines. Details of all these cases are shown in Appendix A of reference 5.

Pitch rates during takeoffs did not exceed 3 deg/s, the peak value being achieved before reaching the maximum load factor.

Takeoffs—Four takeoffs—one at flaps 20 deg and 277.6t (612 000 lb) gross weight and three at flaps 10 deg and gross weights of 244t (538 000 lb), 293.5t (647 000 lb), and 353.8t (780 000 lb) (simulated)—were selected for detailed loads analyses. For two takeoffs, time histories of resultant loads were calculated for the purpose of correlating maximum clearance changes, whenever they occurred, with the aerodynamic loads. For the 353.8t (780 000 lb) takeoff, which was simulated by a pullup maneuver at 305m (1000 ft) above ground level, the analysis was done at the instant the correct airplane lift coefficient was reached.

The flaps 20 deg, 277.6t (612 000 lb) gross weight takeoff was the initial takeoff for the entire test program. Peak load was reached at interrange instrumentation group master clock (IRIG) time 6:41:44. The pitching moment was 37 200 N-m (329 000 in-lb).

The 244t (538 000 lb) takeoff occurred during test 273-10, and the time history covers the IRIG span of 9:44:00 to 9:44:11. Time histories of pitching moment and airflow sensor vane angle* during the takeoff rotation are given in figure 21. The direct relationship of load to flow angle is evident. Also note that the maximum moment for this condition, 45 300 N-m (401 000 in-lb), is considerably higher than the maximum for the flaps 20-deg takeoff.

The 293.5t (647 000 lb) takeoff occurred during test 273-11 between IRIG time 10:13:46 and 10:13:55. The pitching moment time history (fig. 22) shows that the maximum aerodynamic load occurred at IRIG 10:13:52, with a nose-up moment of 48 000 N-m (425 000 in-lb). The load factor was 1.17g.

The simulated high gross weight takeoff occurred during test 273-15 at IRIG 8:13:18. The actual gross weight was 316t (696 500 lb). The simulation was achieved by performing a pullup starting at 346.5 km/h (187 kn) and 1111m (3646 ft) altitude (about 305m [1000 ft] above ground) to produce the same combination of airplane lift coefficient and dynamic pressure that would occur during a 353.8t (780 000 lb) takeoff. (The original intention was to simulate a 372t [820 000 lb] gross weight takeoff. However, insufficient allowance was made for speed reduction due to increasing climb gradient in the pullup maneuver.) The moment at the A-flange was 48 600 N-m (430 100 in-lb).
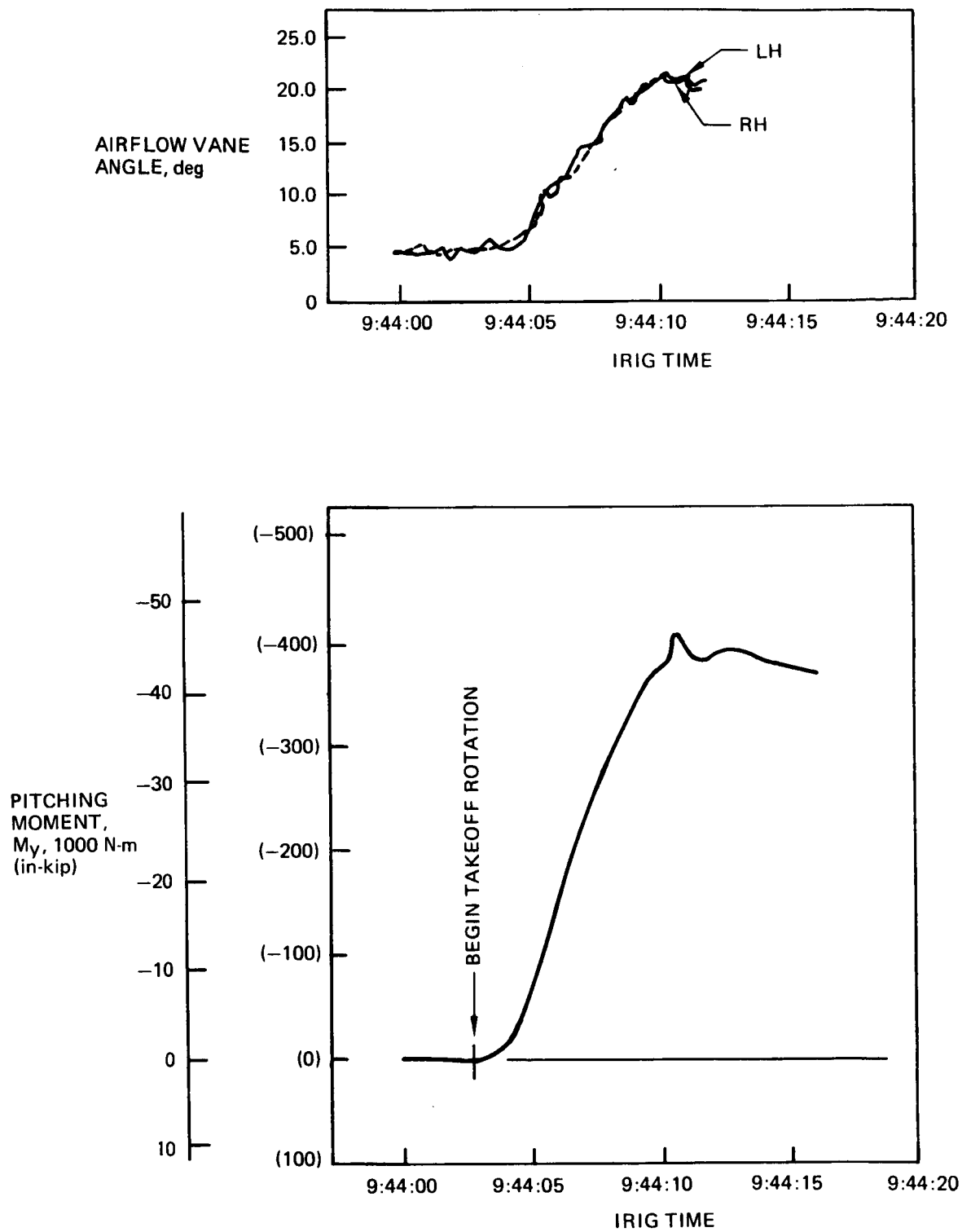
31

Figure 21. *Inlet Pitching Moment Time History, 244t (538 000 lb) Gross Weight Takeoff*
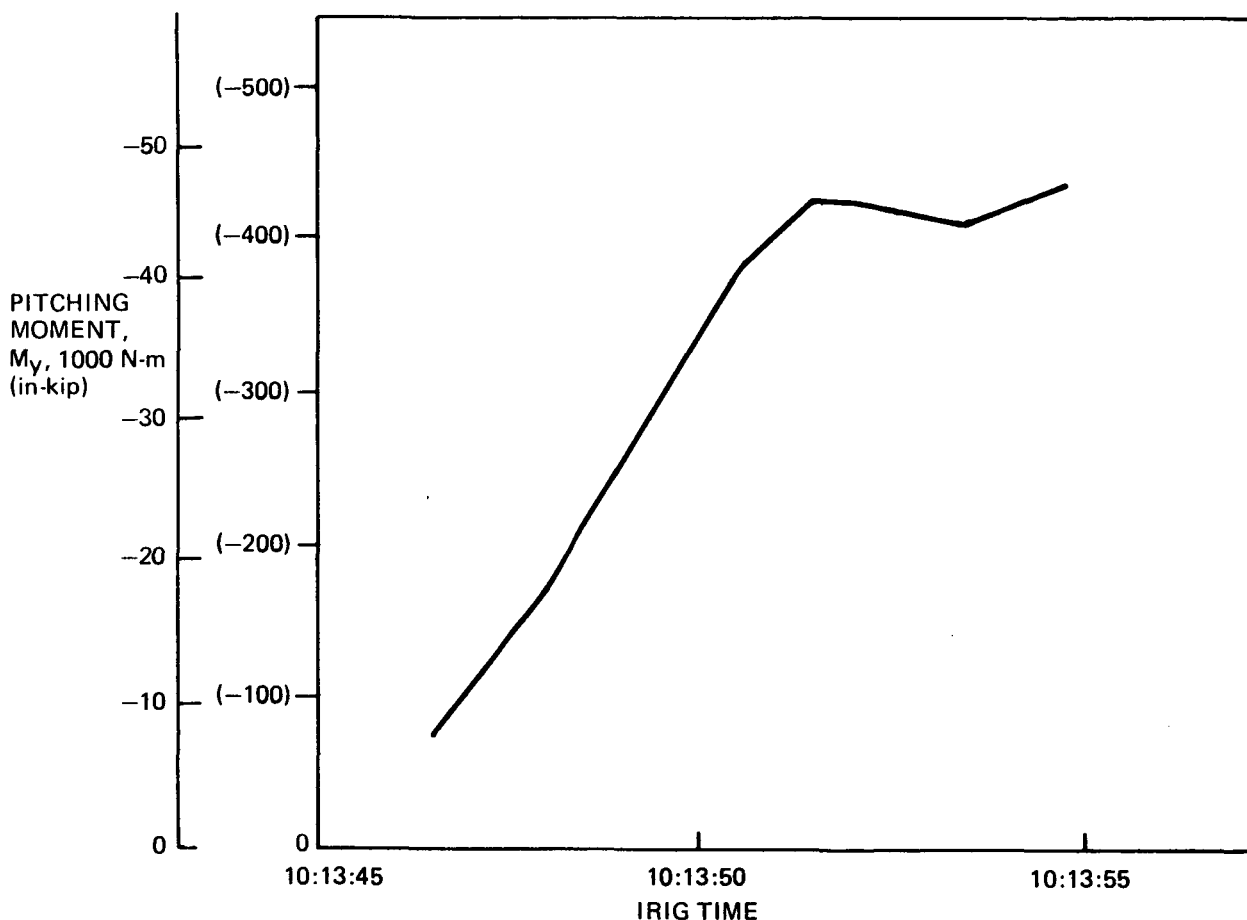
Figure 22. Inlet Airload Moment Time History, 293.5t (647 000 lb) Gross Weight Takeoff

Other Cases—Airloads for conditions other than takeoff were generally much smaller. However, certain cases were analyzed in greater detail because of possible adverse combinations of aerodynamic loads and thermal transients in the engine. Figure 23 shows a time history of the pitching moment at the engine face, engine airflow, and body vane angle for condition 110 (stall warning, 10-deg flaps). The maximum moment, 34 500 N-m (305 000 in-lb), coincided with maximum engine airflow, although the maximum vane angle occurred earlier in the maneuver. The result shows that engine airflow is of comparable importance to angle of attack in determining inlet airloads.

4.2.2 Installed Propulsion System Aerodynamics (IPSA)

Surface static pressures were measured on the right-hand nacelles, pylons, and neighboring wing surfaces in three separate test flights. Data were acquired at M = 0.77, 0.80, and 0.86 during the initial IPSA flight, test 273-09. Instrumentation problems revealed in this test were partially corrected for the second flight, test 273-12, in which data were acquired at the same test conditions. The third flight, test 273-15, was flown primarily to fulfill the remaining Mach 0.91 test condition after the speed restriction imposed by the other Boeing developmental programs was removed.
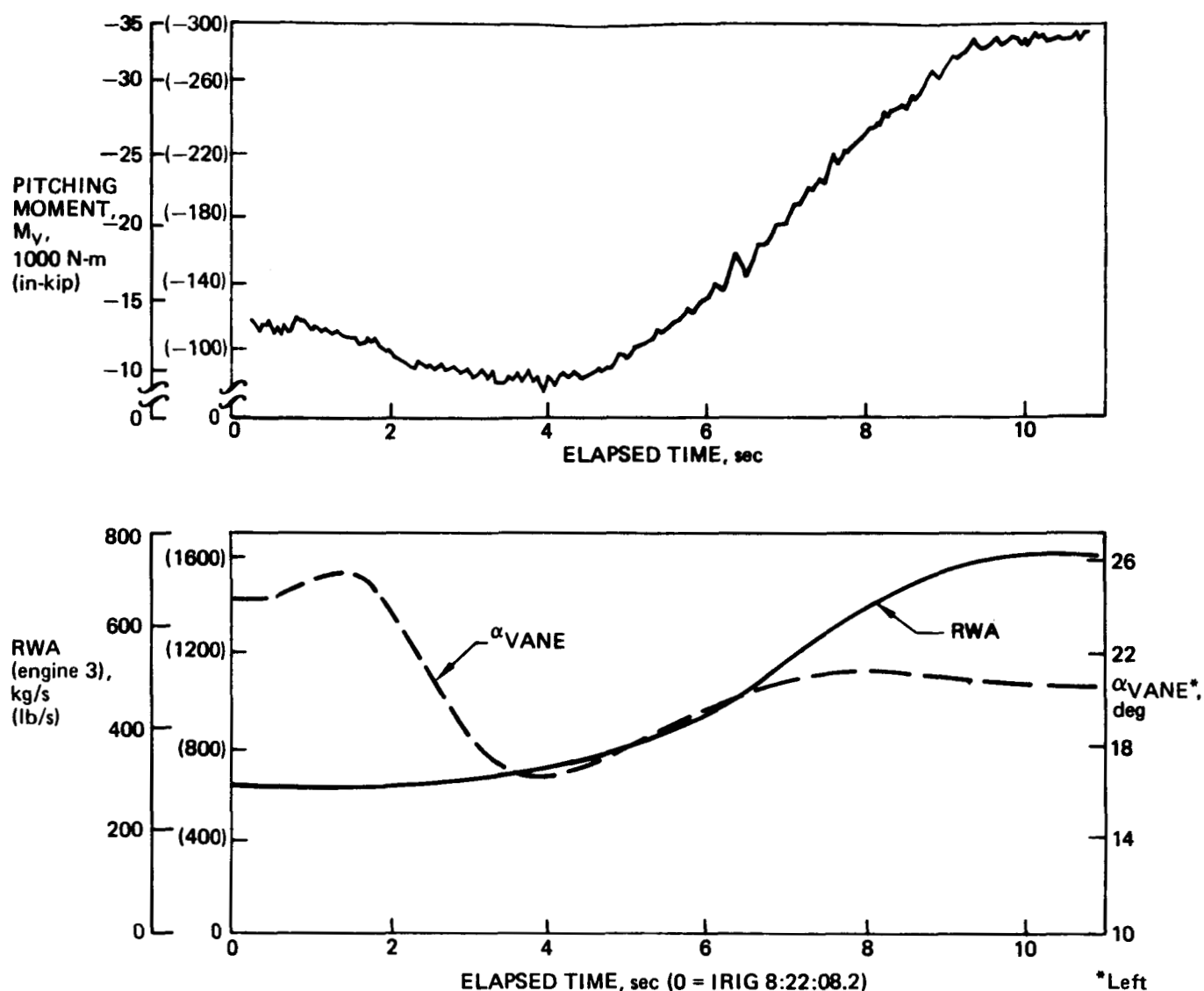
33

Figure 23. *Relation of Inlet Airload Pitching Moment to Angle of Attack and Airflow, Stall Warning Maneuver (Flaps 10)*

Because IPSA testing was intended to create a data base of surface static pressures from a full-scale aircraft, no analysis of the IPSA data was planned or required. Pressure coefficient and local Mach number distributions were plotted for each row of pressure orifices at every condition for each test. Data points considered questionable because of instrumentation problems were removed. The plots, as well as details of the test conditions and data reduction, are presented in Appendix B of reference 5.

---

*The airflow sensor vanes are mounted on both sides of the fuselage near the flight deck. The flow angles indicated by the vanes are influenced by flap setting, wing upwash, body crossflow, and other factors and should not be construed as airplane angle of attack.

5.0 ANALYSIS OF FLIGHT LOADS

5.1 SCOPE

The installed propulsion system aerodynamics (IPSA) portion of this program consisted solely of data gathering. That data will be used in studies of wing/strut/engine interaction to be made and reported in other programs. No analysis of it will be given in this report.

The remainder of this section is devoted to analysis of and commentary on the nacelle aerodynamic and inertial loads.

5.2 AERODYNAMIC LOADS

Figure 24 provides an overview of the relative importance of different flight conditions by comparing their pitching moments in bar chart format. The takeoffs, the flaps 10-deg stall warning maneuver, and the airplane stall are the most severe conditions. No others exceed 35 000 N-m (310 000 in-lb), and the remaining conditions occurring frequently in airline service (climb, cruise, descent, approach, and reverse thrust) are all below 22 600 N-m (200 000 in-lb).
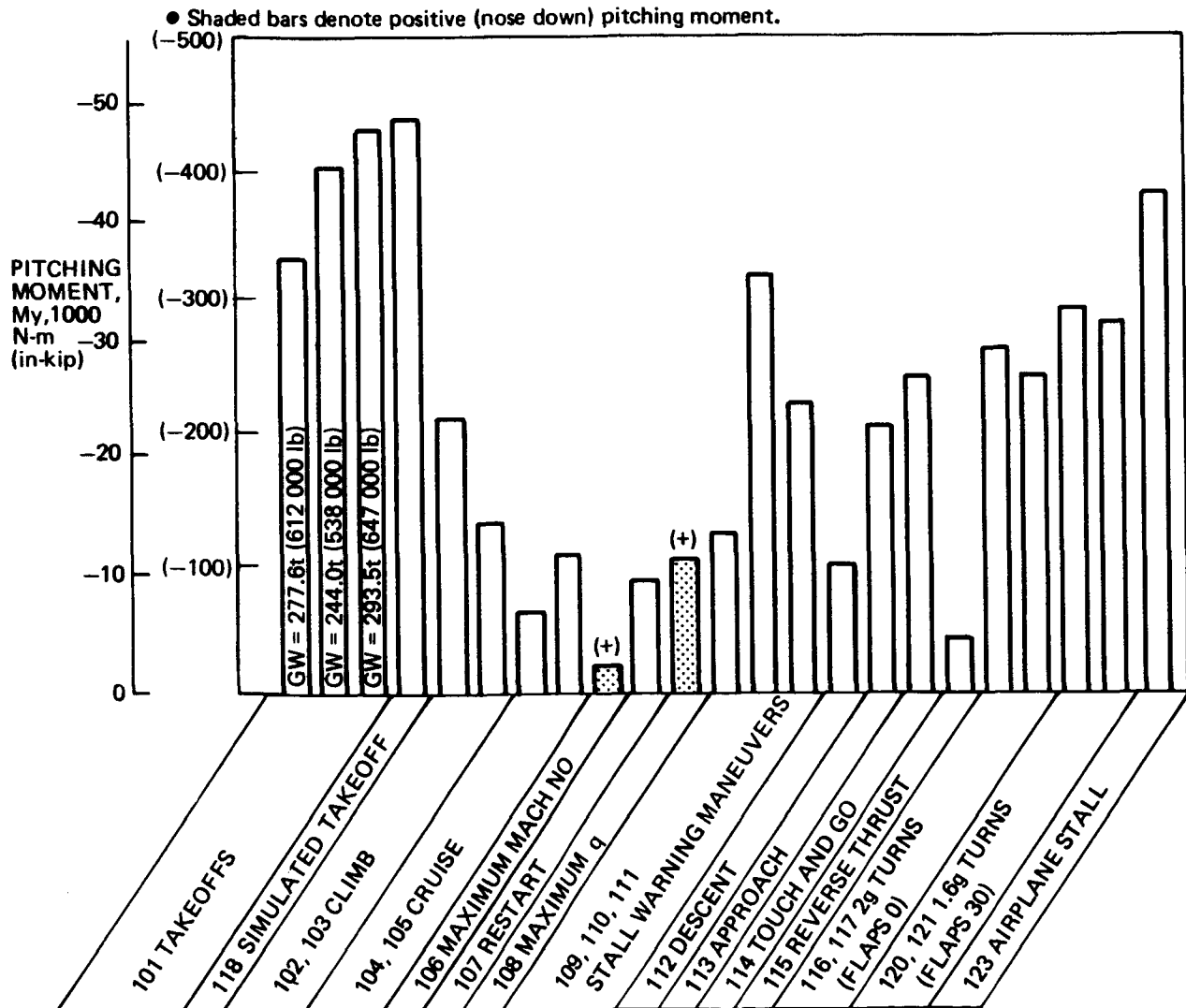

Figure 24. Airload Moment Comparison

35

5.2.1 Takeoffs

The airloads were examined as functions of time during the takeoff maneuver. Figure 25 shows the inlet airloads beginning at the start of ground roll (test 273-15, first flight), continuing through takeoff rotation, and going on to the simulated high gross weight takeoff (symmetrical pullup maneuver) and subsequent recovery. Figure 26 shows key flight parameters (engine airflow, calibrated airspeed, normal acceleration, and altitude) for the same time period.

At first, the largest force component is axial (F_z). The engine, reaching takeoff thrust, draws a high volume of flow around the inlet lip and creates very low pressures there. As the airplane accelerates, the slipstream contraction diminishes and so the axial force declines. A moderate downward vertical force (F_x) is registered, probably because of ground proximity, since the air must enter the inlet from above. The side force (F_y) is small and fluctuating, showing the influence of somewhat variable wind across the runway. (The pitching and yawing moments track the vertical and side forces closely and will not be discussed separately.)

Just before takeoff rotation, at 53 sec elapsed time, the relative wind is dominated by the airplane's forward speed at 287 km/h (155 kn), but the inlet is closely aligned to it and
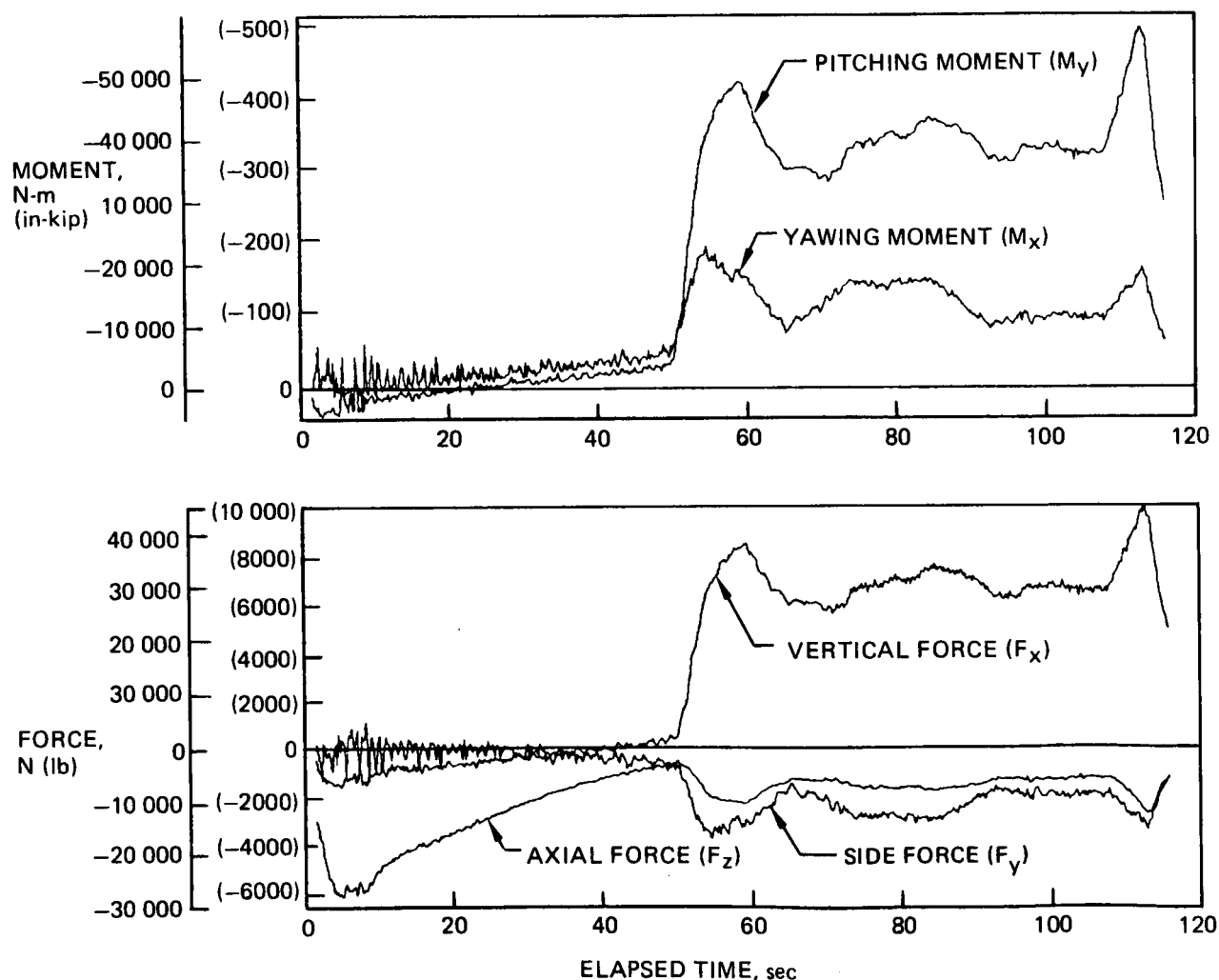

Figure 25. Airload Time Hsitory for Takeoff and Condition 118 Pullup Maneuver
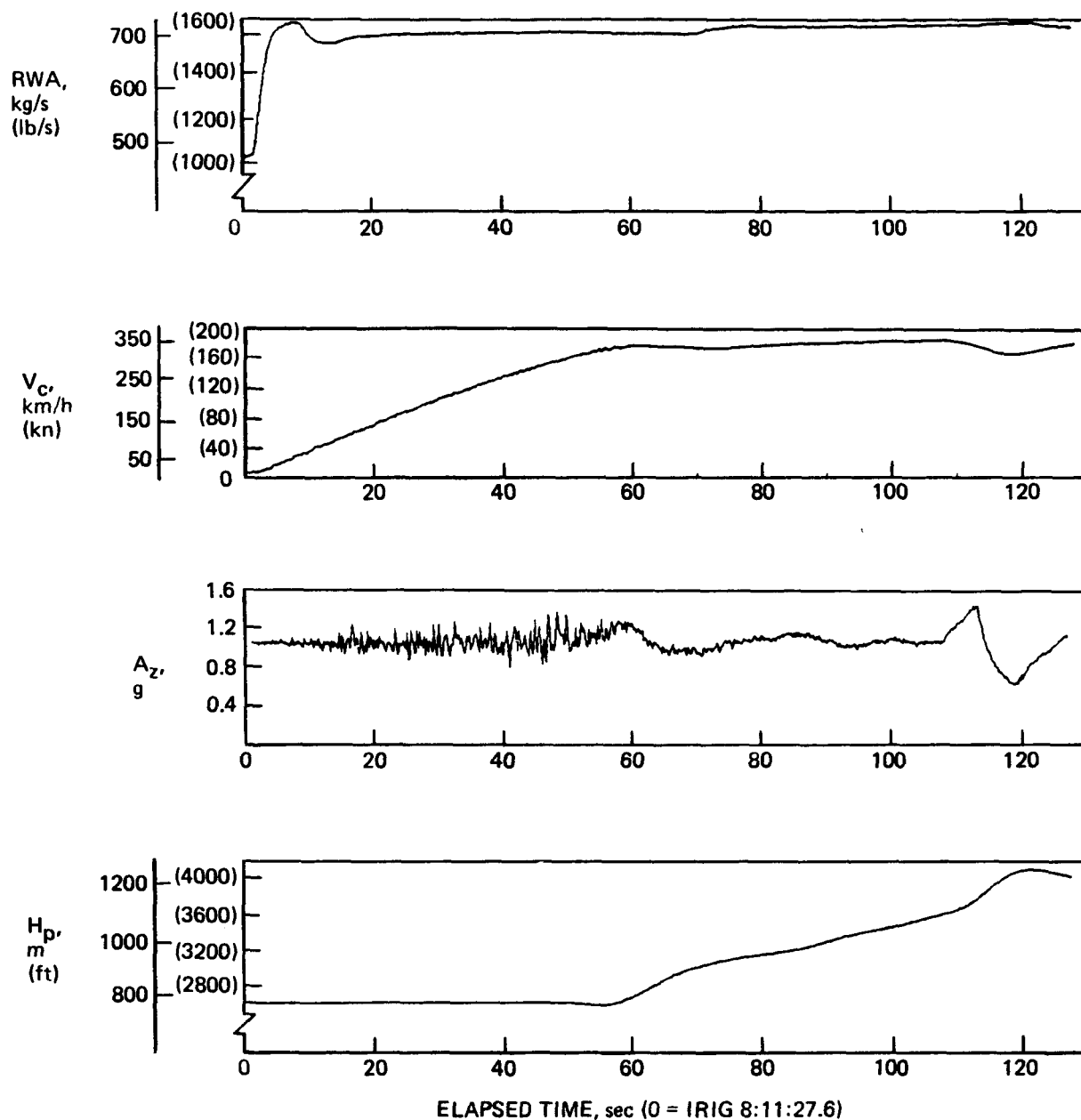
36

Figure 26. Flight Parameters for Takeoff and Condition 118 Pullup Maneuver

forces are very low. As the airplane rotates, significant vertical and side forces appear. The vertical shear rises to a maximum of nearly 35 000N (7870 lb) as the pilot pulls up at more than 1.2g's to lift the airplane off. A reduction in vertical shear follows in the period from 60 to 64 sec, coincident with the return of the vertical acceleration to about 1.0g.

The side force builds up to an outboard-directed maximum of just under 17 000N (3820 lb) at approximately 54 sec, fully 5.5 sec before maximum vertical load is reached. The reason for the difference in timing of peak loads is that an angle of sideslip (local to the inlet) is required to generate side force and yawing moment. A lateral component of flow creating such a sideslip is induced by the circulation pattern about the lifting sweptback wing. This flow is augmented by a contribution due to ground effect; the trailing-edge flaps restrict passage of air beneath the wing, forcing it outboard. When the airplane lifts

37

off, the tight clearance below the trailing edge is relieved, and only the outflow due to the basic circulation pattern remains. The side force and yawing moment therefore decline to the level associated with the lift-induced flow alone, while the vertical force and pitching moment continue to rise. (Note that in the case of the simulated takeoff, flown out of ground effect, the peak vertical and side loads are simultaneous at 113.5 sec elapsed time.)

Shortly after settling down to 1g flight, the pilot would normally be expected to accelerate and retract the flaps. In this case, however, the flight test plan called for a symmetrical pullup maneuver to be executed 305m (1000 ft) above ground level, with flaps still at 10 deg and at a speed appropriate to a 372t (820 000 lb) takeoff, 346 km/h (186 kn) calibrated airspeed (CAS) . Therefore, in the period from 64 to 115 sec elapsed time, the pilot accelerates only slightly, and the loads remain at roughly the same level except for an increase when the engine thrust is adjusted upward at 72 sec.

The simulated high gross weight takeoff (condition 118) was a selected instant during the pullup maneuver between 108 and 112.5 sec. The intention was simultaneously to achieve a dynamic pressure and an angle of attack appropriate to the 372t (820 000 lb) takeoff at the peak-g condition. Because the actual gross weight was only 316t (696 000 lb), a higher g level was needed to match the airplane lift coefficient to the nominal value. The absence of ground effect, however, implied that the angle of attack at the nominal lift coefficient (C_L) would be exaggerated, so a somewhat reduced C_L was selected.

Because of speed bleedoff during the pullup, when the airplane reached the desired C_L, the dynamic pressure had fallen below the value appropriate to 372t (820 000 lb). It was determined that the match was achieved at 340.2 km/h (184 kn) CAS, corresponding to a gross weight of 354t (780 000 lb), at 110.4 sec elapsed time.

Figure 27 shows the pressure coefficients measured at the instant of maximum airload during the 244t (538 000 lb) gross weight takeoff (condition 101) at the top and bottom rows of pressure taps (θ = 0 and 180 deg) of engine 3. They are plotted against nondimensional distance measured perpendicular to the highlight plane. In this format, a difference in pressure at a given value of the abscissa is directly indicative of a contribution to vertical force.

In this condition, the flow is much faster inside than outside the inlet. As a result, the interior pressures on both the top and bottom are well below ambient. The effect of angle of attack is to require such a severe acceleration around the lower lip that the flow becomes supersonic (C_p for Mach 1.0 is -11.24 at M_∞ = 0.239). The minimum measured pressure corresponds to a local Mach number of 1.33, just inside the lower lip. An abrupt pressure rise to the subsonic level indicative of a shock follows. This is followed by a short zone of approximately constant pressure, probably a separation bubble. Diffusion then proceeds fairly smoothly to the engine face. Pressures at the top row of taps are well below ambient, but much higher than those at the bottom row.

On the outside, pressures are not dominated by engine effects, but rather by external aerodynamic influences. As a result, differences from ambient are much less dramatic than they are on the inside. (In the forward 20% of the inlet, the average difference between the pressures on the inside is more than five times the average difference of the outside pressures.) Therefore, most of the aerodynamic load is attributed to the interior pressures.

Figure 28 shows the pressure coefficient plotted versus circumferential position in the first 10% of the inlet interior. A roughly consinusoidal variation prevails, but it is
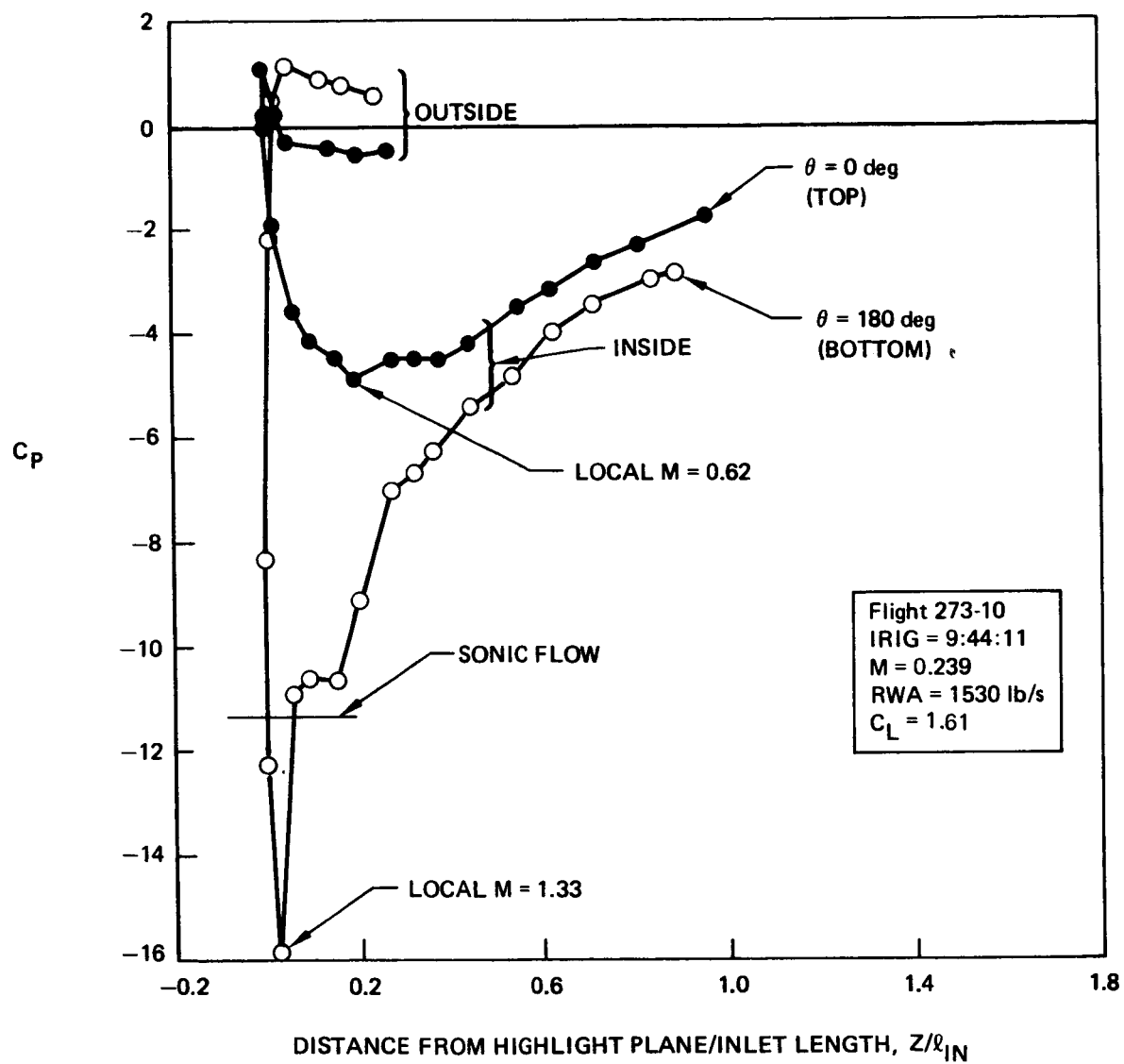
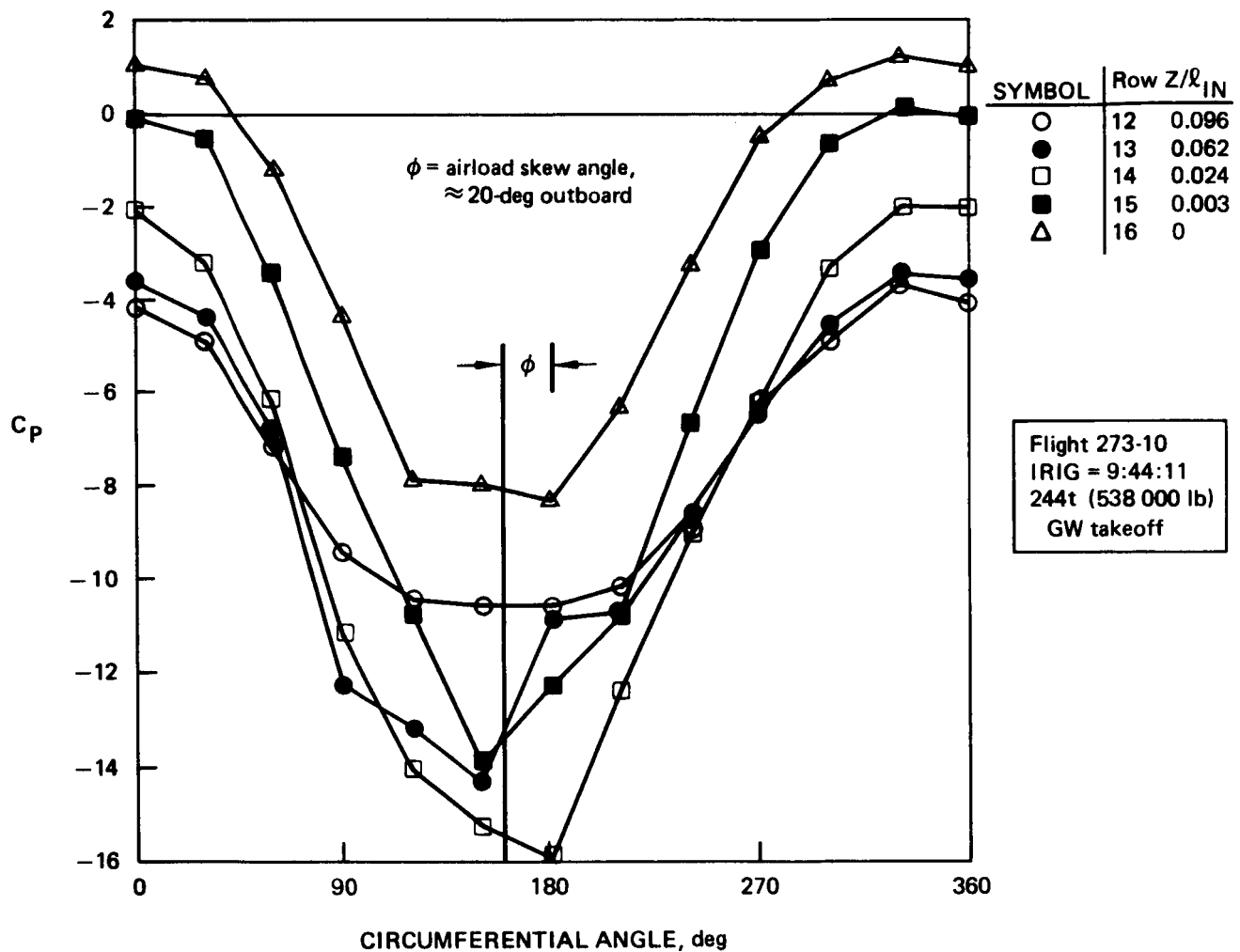*Figure 27. Pressure Coefficient Distribution, 244t (538 000 lb) Gross Weight Takeoff, Engine 3*

Figure 28. Circumferential Variation of Pressure Inside Inlet, Engine 3

displaced toward the inboard side of the inlet by about 20 deg. This skewing of pressures agrees with the ratios of side force and yawing moment to vertical force and pitching moment that are -0.405 and 0.380 (corresponding to 22.1 deg and 20.8 deg, respectively).

Because it was farther outboard, engine 4 was expected to operate at slightly lower angle of attack than engine 3 because of aeroelastic twist. Slightly lower loads therefore were anticipated. Figure 29 compares pressures at the 180-deg circumferential location for
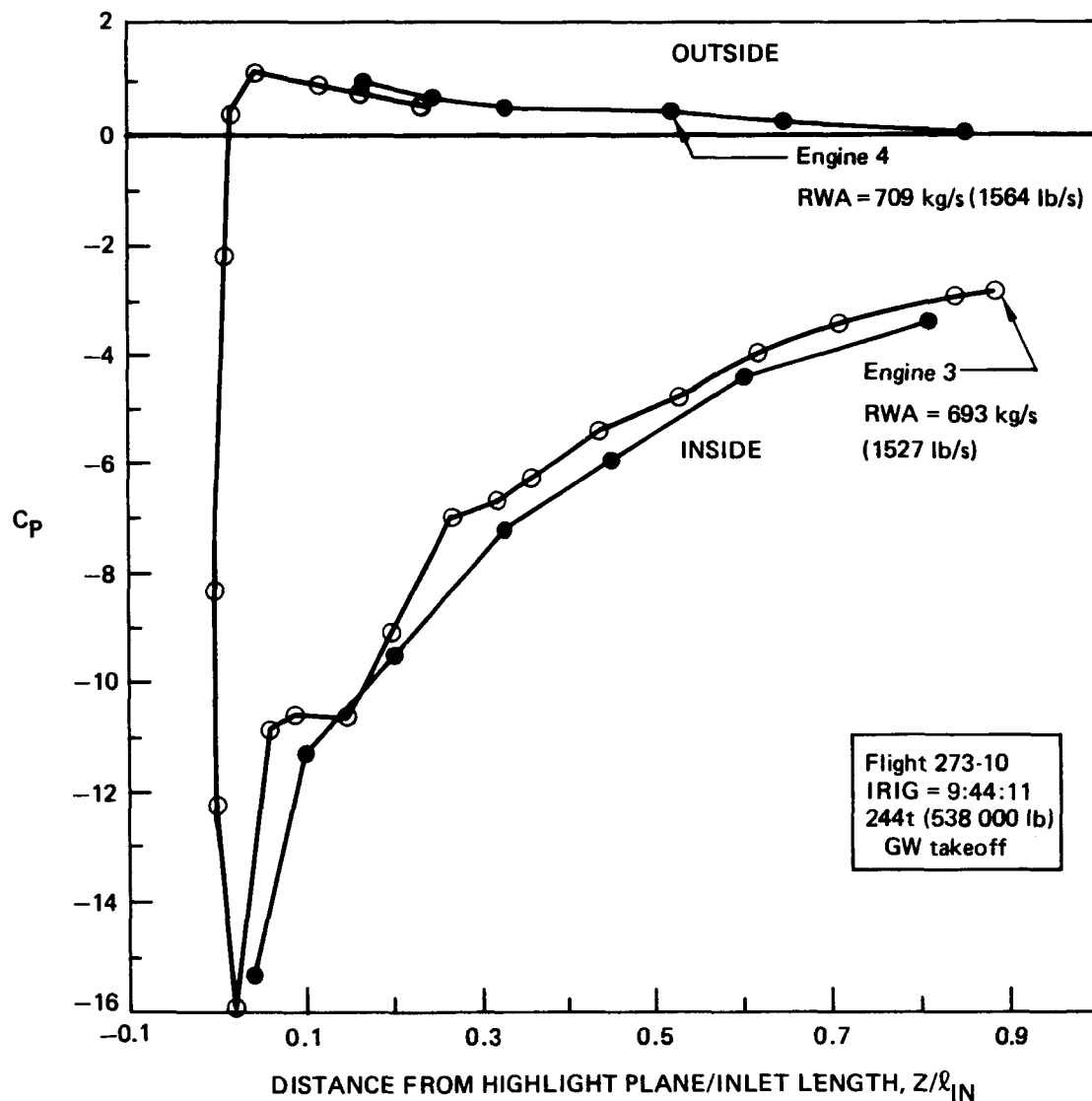

Figure 29. Pressure Comparison, θ = 180 deg, Engines 3 and 4

engines 3 and 4 at the same flight condition. In this case, a slightly greater load is indicated by the lower pressure coefficients for engine 4. If allowance is made for the fact that engine 4 was running at 2.4% higher airflow, however, the pressures indicate that the angles of attack are nearly equal.

Note that the airloads were substantially lower for the flaps 20-deg takeoff than for any of the flaps 10-deg takeoffs because the higher flap deflection reduces the angle of attack at liftoff. Inlet airloads can therefore be reduced, when operational requirements permit, if the use of the 10-deg flap setting can be avoided.

41

5.2.2 Stall Warning Maneuvers

The only condition in the acceptance flight profile where the inlet airloads approach those at takeoff is the stall warning maneuver at flaps 10 deg. This maneuver is a functional check of the stick shaker system, which warns the pilot that he is approaching stall. It is carried out by gradually reducing airspeed at an altitude of approximately 5200m (17 000 ft) until the warning system is actuated. The power setting, and therefore the engine airflow, are low in this condition because of the requirement to lose airspeed.

After the warning system has started shaking the control column, the pilot recovers by pushing the nose down and adding power. It is only as the engine speed builds up that the airloads reach significant levels, as shown in figure 23 in section 4.2.1.1. Airloads could therefore be reduced if the power increase were delayed until a higher speed was reached.

The fact that the stall warning checks at flaps 0 and flaps 30 deg both resulted in lower maximum airloads than the flaps 10-deg maneuver requires explanation. In all three cases, maximum loads were reached when the engine reached its highest power level, but the angle of attack was highest in the flaps 10-deg condition. At flaps 0 deg, the leading-edge flaps are not deployed, and the wing stall angle is relatively low. At flaps 10 deg, the leading-edge flaps have increased the stall angle considerably, although the C_L at any given angle (below stall) is changed little. Trailing-edge flap deflection progressively reduces the stall angle. At flaps 10 deg, the reduction of stall angle due to the trailing-edge flaps is still overshadowed by the increase due to leading-edge flaps. By the time the flaps reach 30 deg, however, the stall angle has been driven back to around the flaps 0-deg value.

5.2.3 Airplane Stall

Condition 123, a power-on airplane stall, was considered of interest because the angle of attack was the highest developed in any condition flown. Figure 30 shows pressure coefficients plotted against arc length measured from the highlight.* Although the freestream Mach number was only 0.207, an extensive region of supersonic flow is evident, reaching a local maximum of Mach 1.65. Despite the combination of high power setting and high angle of attack, the air loads were lower than those observed for flaps 10-deg takeoffs because the maneuver was carried out at 2743m (9000 ft) altitude, and the dynamic pressure was correspondingly low.

5.2.4 High-g Turns

Four turns were performed to investigate inertial load (acceleration and gyroscopic torque) effects on the engines. The inertial loads were accompanied by aerodynamic forces of somewhat lower magnitude than those observed in the takeoffs and the flaps 10-deg stall warning maneuver.

---

*This format was selected for plots in which C_p's are shown for more than two θ's at once to prevent illegibility due to crowding of data points near the highlight. Note that since arc lengths are defined to increase going forward on the inside, interior pressure distributions appear reversed, compared with plots against axial distance (x).
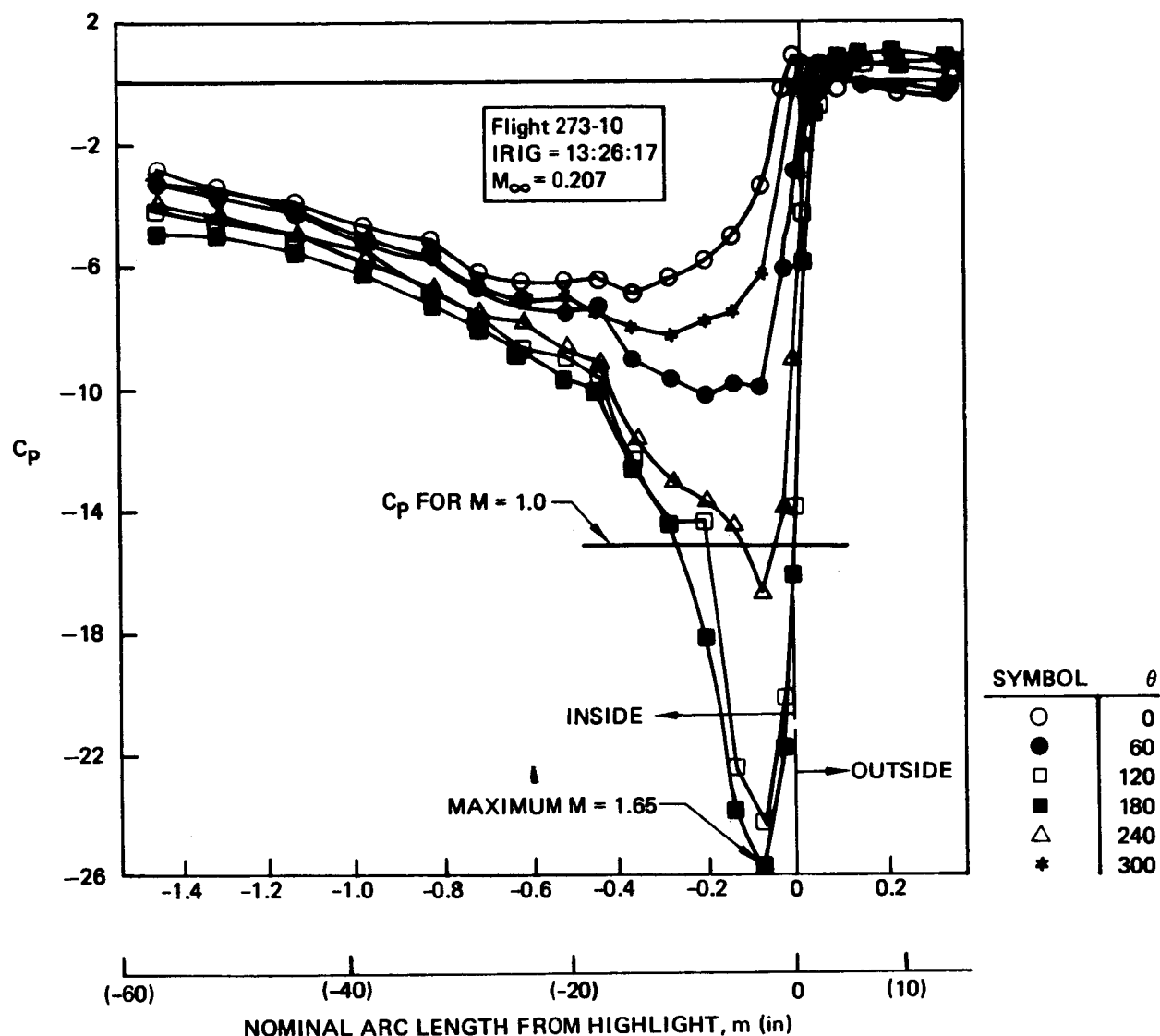
Figure 30. Inlet Pressures, Airplane Stall, Condition 123, Engine 3

5.2.5 Other Conditions

Near cruise speed, quite different pressure distributions prevail on the inlet and cowl. Figure 31 shows Cp's in low Mach cruise (condition 105). Note that the pressures inside the inlet are mostly higher than ambient, because the engine ingests a smaller streamtube of air, which is therefore slowed to lower than freestream velocity. Note also that the Cp variations are an order of magnitude smaller than was the case at low speed. As a result, loads are much smaller and mostly register on the outside of the cowl.

Similar pressure distributions were observed for late climb, high Mach cruise, maximum Mach number, engine restart, maximum dynamic pressure, and descent (conditions 103, 104, 106, 107, 108, and 112), and loads were small in all cases. Because of the speed restriction on the JT9D-7R4 engine and nacelle, the maximum dynamic pressure condition was simulated in a pushover (less than 1.0g) maneuver to achieve aerodynamic similarity, matching the C_L of 694.5 km/h (375 kn) equivalent airspeed (EAS) flight at 6100m (20 000 ft) altitude at an actual altitude of 7470m (24 500 ft) and airspeed of 667 km/h (360 kn) EAS. The low airplane angle of attack, together with the 4-deg inlet droop, resulted in a net negative inlet angle of attack and a nose-down pitching moment.
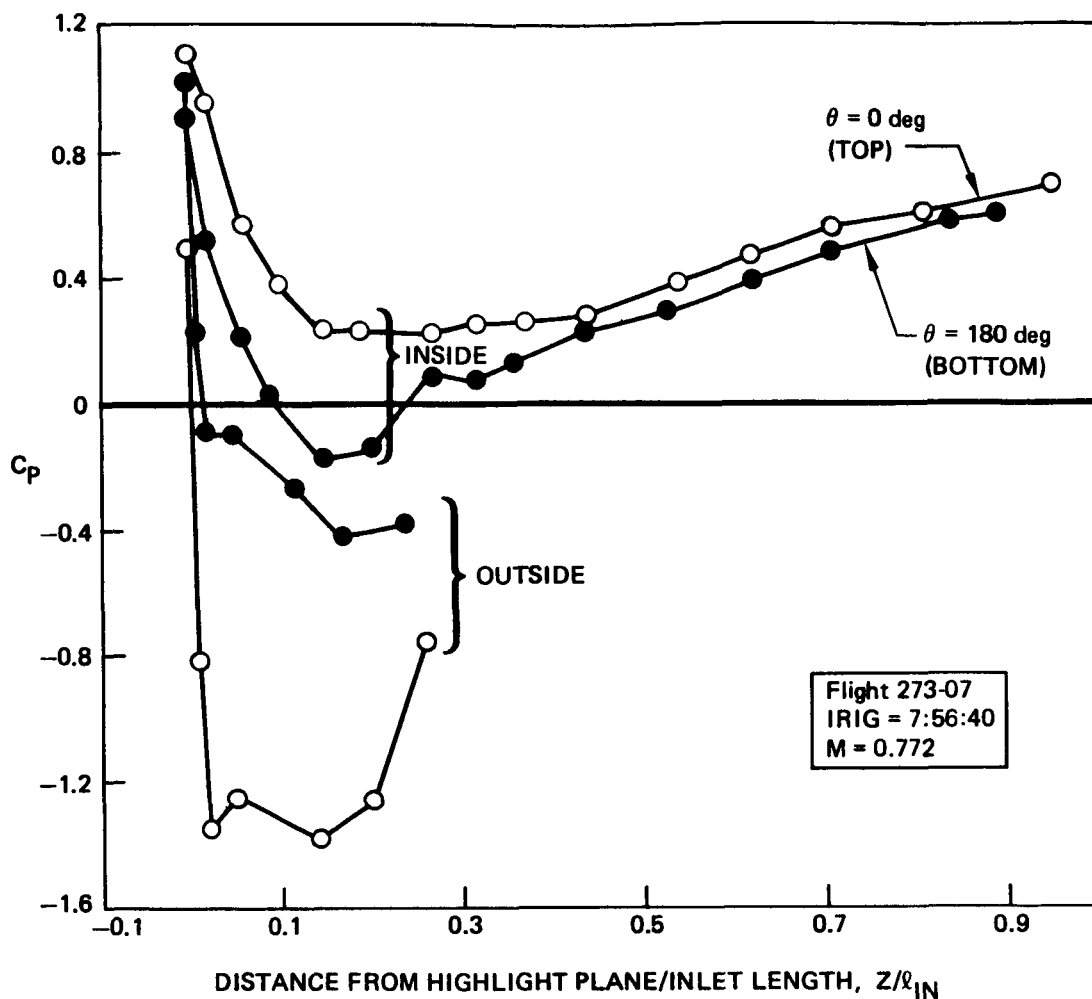
43

Figure 31. Inlet Pressure Coefficient Distributions, Low Mach Cruise, Condition 105, Engine 3

Early climb, approach, and the touch-and-go landing (conditions 102, 113, and 114) showed pressure distributions more like the low-speed conditions, but very moderate airloads. Thrust reverse (condition 115) produced small airloads because the angle of attack was near zero.

5.2.6 Gust Sensitivity

Gusts affect both aerodynamic and inertial loads, which must be considered simultaneously. The aerodynamic load arises directly from the change of inlet angle of attack associated with the gust component of the relative wind. The inertial load is produced by the airplane's motion in response to the gust. No appreciable turbulence was encountered in the flight program, so this combined effect was not observed. Nevertheless, it was possible to establish the sensitivity of the inlet aerodynamic loads to angle of attack changes caused by gusts. In the simulated maximum q pushover maneuver, loads were measured over a range of airplane angles of attack. From these data it was determined that the derivative of pitching moment with angle of attack at that Mach number and altitude was 9912 N-m (87 736 in-lb) per degree.

44

To put this figure in perspective, consider a maximum airspeed condition, 694.5 km/h (375 kn) EAS (747 maximum operating airspeed) at 6096m (20 000 ft) altitude. (This condition was chosen as a "worst plausible" case, much faster than economical climb, cruise, or holding speeds.) At this altitude, an 11-m/s (36-ft/s) gust can be expected about once in 800 hr of flying (ref. 6). The true airspeed at this EAS and altitude is 300 m/s, so an 11 m/s gust would produce an angle of attack change of 2.1 degrees. Allowing for the 8.5% higher actual (as opposed to simulated) dynamic pressure, a pitching moment change of 22 600 N-m (200 000 in-lb) would be caused by the gust. This moment is about half of the nose-up pitching moment to be expected routinely at takeoff.

5.3 GENERALIZED AIRLOADS

To apply the results of this program to other aircraft/engine combinations, it is necessary to express the airloads in nondimensional form and to relate them to parameters that are not peculiar to the 747 equipped with JT9D-7A engines.

Following the usual aerodynamic practice, forces will be nondimensionalized by dividing by dynamic pressure times a reference area. The inlet highlight area was selected for this purpose, so

$$C_{F_{(\ )}} = \frac{F_{(\ )}}{\frac{1}{2}\rho_\infty V_\infty^2 A_H}$$

where the empty parentheses indicate a subscript x or y, for vertical or side force, as indicated on figure 20. Moments are nondimensionalized using highlight area times inlet length (distance from the highlight plane, to the A-flange plane, measured along the inlet centerline). That is,

$$C_{M_{(\ )}} = \frac{M_{(\ )}}{\frac{1}{2}\rho_\infty V_\infty^2 A_H \ell_{IN}}$$

In the present case, A_H is 4.364m^2 (6764 in^2) and ℓ_{IN} is 1.476m (58.1 in).

The airload coefficients depend on the inlet angles of attack and sideslip (α_{IN} and β_{IN}) and on airflow. The latter has been nondimensionalized as the ratio of the remote streamtube area to the highlight area and denoted by airflow parameter (AFP). That is,

$$AFP = \frac{WA}{\rho_\infty V_\infty A_H g}$$

If the flow were incompressible and inviscid and if local nonuniformities due to the airplane were negligible, then the pressure coefficient at any point on the inlet or cowl would be *wholly* determined by α_{IN}, β_{IN}, and AFP. In practice, since the loads of interest all occur in a small Mach number range (0.22 to 0.32), it is safe to ignore compressibility effects despite the fact that the inlet flow is transonic. Viscosity (Reynolds number) effects can also be neglected, since all big high bypass ratio turbofans are of comparable scale. It follows that the force and moment coefficient data can be understood in terms of the three parameters α_{IN}, β_{IN}, and AFP.

α_{IN} and β_{IN} cannot be measured in flight, since they are defined as the angles (in the vertical and horizontal planes, respectively) between the inlet centerline and the flow direction at the highlight plane that would prevail if the engine/nacelle were not there. They can be measured in nacelle-off wind tunnel flow surveys or inferred from comparison of inlet lip pressures to isolated powered model nacelle data. In either case, they are

45

subject to considerable uncertainty because of scale effects. (Airplane C_L versus α may be different at model scale, especially at high α's, so the flow pattern will not match. In the case of model nacelles, the interior flow will usually separate at a lower angle than at full scale.)

In the present study, α_{IN} data based on nacelle-off flow surveys was used. No data on β_{IN} was available, so no attempt was made to generalize the side force and yawing moment data. (The ratios of side force to vertical force and of yawing moment to pitching moment are fairly closely grouped around 0.4 for all the takeoffs. This is configuration dependent, however, and will not necessarily apply to aircraft other than the 747.)

To ensure the best available statistical basis, 31 low-speed flight conditions (including eight takeoffs not included in tables 1 and 4 and six points in the condition 118 pullup maneuver) were analyzed. They are listed in table 5.

The function used to fit the data was of the form

$$C_{(\,)} = K_o + K_1 \, \alpha_{IN} + K_2 \, AFP + K_3 \, \alpha_{IN} \, AFP$$

This is called a "ruled surface" function because of the linearity of $C(\,)$ with either variable.

The coefficients in the equation were determined to minimize the rms error between the fitting function and the data of table 5, giving

$$C_{F_x} = 0.606 + 0.0782 \, \alpha_{IN} + 0.779 \, AFP - 0.01435 \, \alpha_{IN} \, AFP$$

with an rms error of 0.08 and a maximum error of 0.24, and

$$C_{M_y} = 0.777 - 0.0431 \, \alpha_{IN} - 0.871 \, AFP - 0.00563 \, \alpha_{IN} \, AFP$$

with an rms error of 0.07 and a maximum error of 0.20. Figures 32 and 33 show the fitted values plotted against measured values and the associated error.

It is reasonable to ask how closely an inlet must match the geometry of the 747/JT9D-7A design for the force and moment coefficient data presented here to be applicable. No comparable measured loads are available for any other inlet, but a comparison can be made of loads calculated from theoretical pressure distributions. Figure 34 shows the NAIL inlet profile and the profile of another inlet designed for a different airframe and a different manufacturer's engine. (Both are approximately to scale.) An inviscid compressible flow finite-difference analysis was used to compute pressures on both, and the results were integrated to give airload coefficients. Figure 35 is a comparison of the theoretical airload coefficients for the two inlets at AFP and α_{IN} values typical of takeoff.

The derivative of C_{M_y} with α_{IN} is almost perfectly matched, while the absolute value is offset by approximately 3%. Similar agreement was obtained for C_{F_x}. Therefore, it can be expected that use of the nondimensional NAIL loads for inlets differing in the same degree would give comparable agreement.

The development of pressure distribution data for this comparison permitted evaluation of how well inviscid compressible flow theory models the real inlet behavior for load

Table 5. Low-Speed Aerodynamic Force and Moment Coefficients

Condition	Test (237–)	IRIG time	Airplane C_L	Flaps	IGE/OGE	α_{IN}	M_∞	AFP	C_{F_x}	C_{M_y}
101 TAKEOFF	7	6:41:44.15	1.597	20	—	17.300	0.250	1.602	1.494	-1.422
TAKEOFF	9	9: 4:42.70	1.574	10	—	20.400	0.239	1.658	1.863	-1.770
"	9	16: 6:43.20	1.510	10	—	19.100	0.235	1.680	1.705	-1.692
101 TAKEOFF	10	9:44:10.60	1.612	10	—	21.900	0.239	1.647	1.996	-1.913
" "	10	9 44 13.90	1.489	10	O	19.600	0.246	1.609	1.806	-1.723
101 TAKEOFF	11	10:13:50.60	1.485	10	—	18.600	0.253	1.560	1.570	-1.472
" "	11	10:13:51.60	1.527	10	—	19.600	0.254	1.553	1.945	-1.796
" "	11	10:13:54.80	1.590	10	O	22.400	0.260	1.522	1.961	-1.753
TAKEOFF	12	8:50:42.00	1.673	10	—	23.600	0.241	1.627	2.022	-1.908
"	12	9:23:58.00	1.565	10	—	20.500	0.245	1.620	1.851	-1.786
"	12	10:14:20.00	1.560	10	—	20.800	0.233	1.698	1.786	-1.749
"	14	7:57:38.00	1.839	10	—	26.000	0.213	1.803	2.209	-2.223
"	14	8:12:22.00	1.384	10	—	18.000	0.242	1.629	1.568	-1.481
118 ACT TAKEOFF	15	8:12:24.10	1.546	10	O	20.000	0.276	1.455	1.637	-1.488
118 SIM HGWTO	15	8:13:18.00	1.489	10	O	18.600	0.296	1.395	1.562	-1.386
" "	15	8:13:18.70	1.504	10	O	20.800	0.294	1.402	1.669	-1.489
" "	15	8:13:19.20	1.538	10	O	21.400	0.293	1.406	1.789	-1.586
" "	15	8:13:19.40	1.594	10	O	22.500	0.291	1.414	1.830	-1.647
" "	15	8:13:19.80	1.650	10	O	23.500	0.290	1.418	1.892	-1.683
" "	15	8:13:20.20	1.628	10	O	22.800	0.288	1.427	1.837	-1.681
123 STALL	10	13:26:15.00	2.404	30	O	35.000	0.210	1.889	2.535	-2.643
109 STALL WRNG	7	8:18:58.00	0.848	0	O	11.200	0.389	1.094	0.941	-0.721
110 "	7	8:22:07.00	1.463	10	O	20.000	0.299	0.555	1.193	-0.583
" "	7	8:22:26.00	1.286	30	O	17.000	0.347	1.250	1.387	-1.168
111 "	7	8:24:48.30	1.541	30	O	11.700	0.251	1.312	1.049	-0.885
" "	7	8:24:51.85	1.780	0	O	16.800	0.270	1.574	1.489	-1.440
116 HIGH g TURN	10	13:33:59.00	0.632	0	O	7.150	0.483	0.924	0.575	-0.370
117 HIGH g TURN	10	13:41: 2.00	1.857	30	O	18.500	0.260	1.537	1.559	-1.448
120 "	15	11: 4:03.00	0.770	0	O	9.300	0.476	0.715	0.657	-0.355
121 "	15	11: 7:25.00	1.925	30	O	20.000	0.266	1.402	1.492	-1.339
" "	15	11: 7:27.40	2.030	30	O	22.200	0.265	1.405	1.694	-1.522

prediction purposes. The NAIL C_{My} curve-fit functions for AFP = 1.5 are also shown on figure 35. The derivative of C_{My} with i_N is substantially lower, although the magnitude is in reasonable agreement. In the case of C_{Fx}, however, agreement is worse. The test data show a C_{Fx} level substantially higher than the theoretical values.
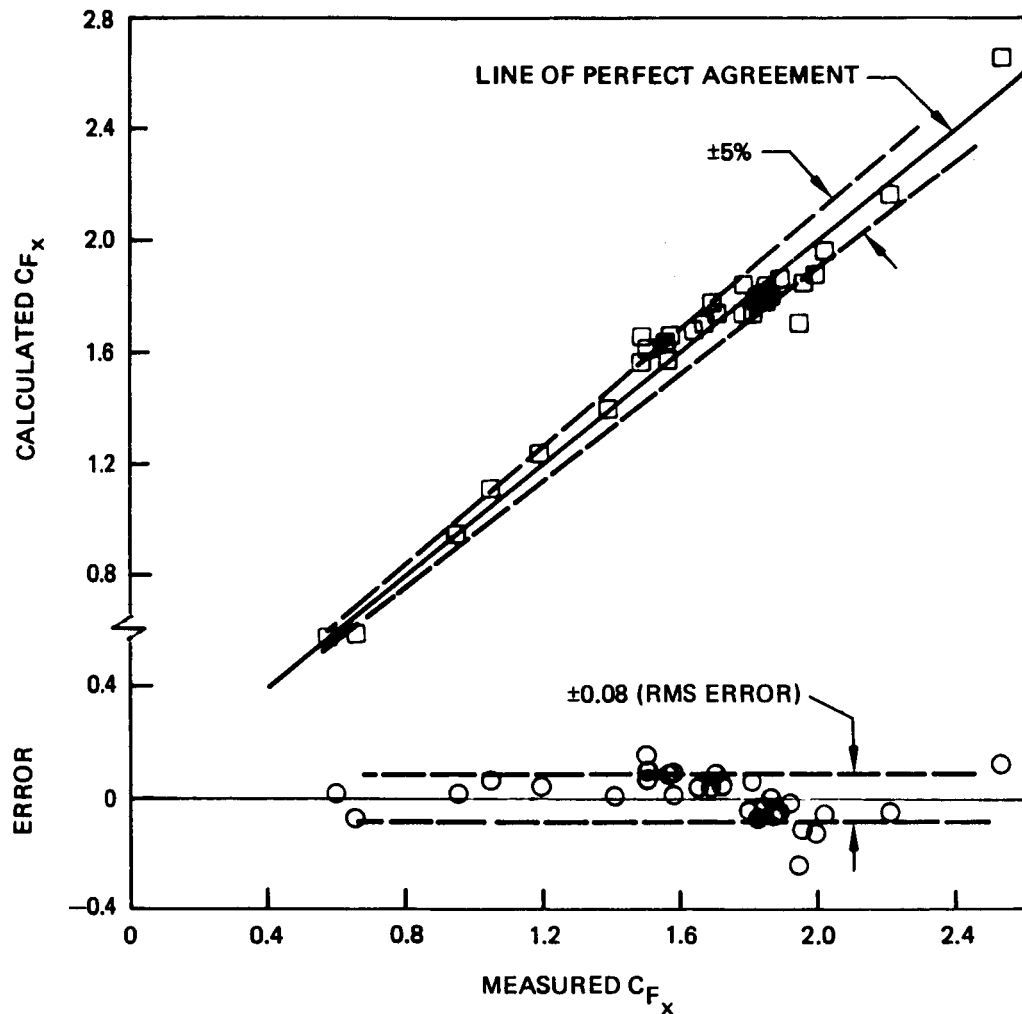

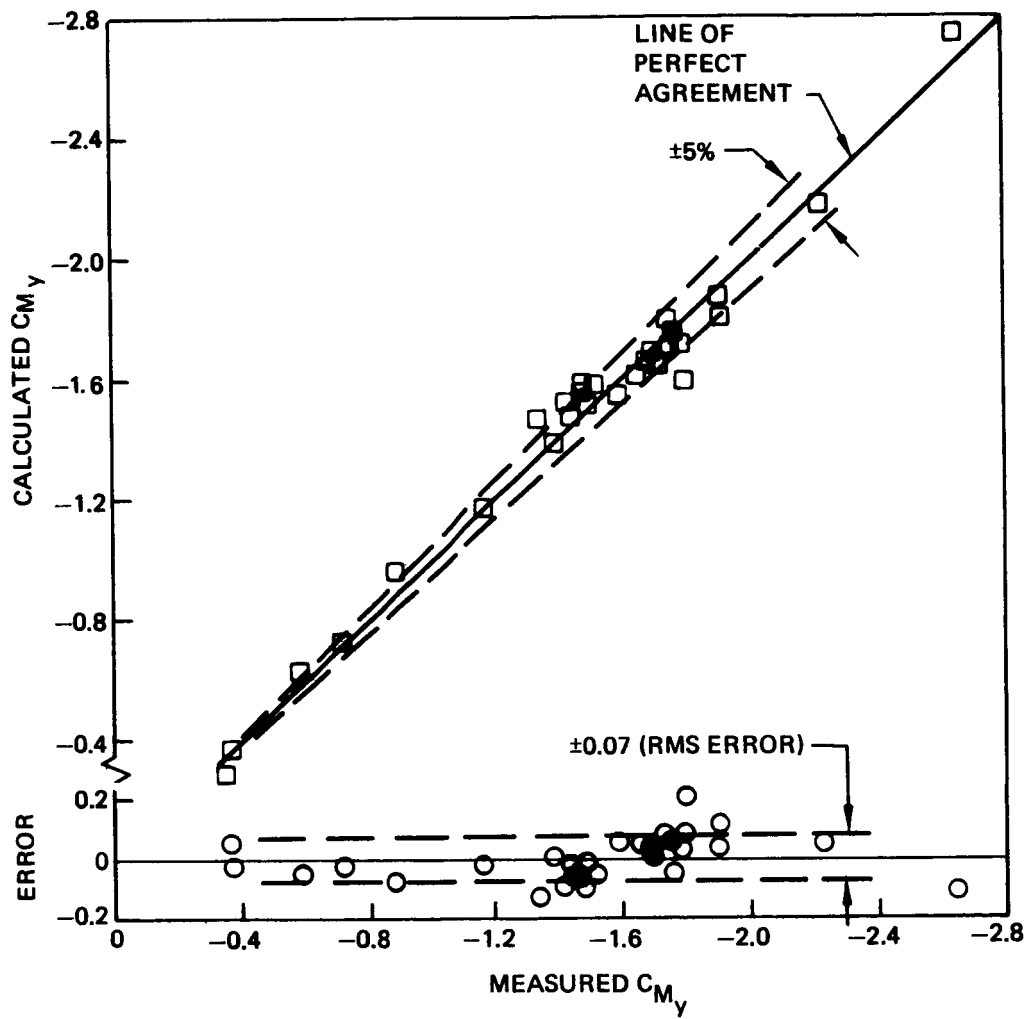Figure 32. Ruled Surface Fit to Vertical Force Coefficient

48

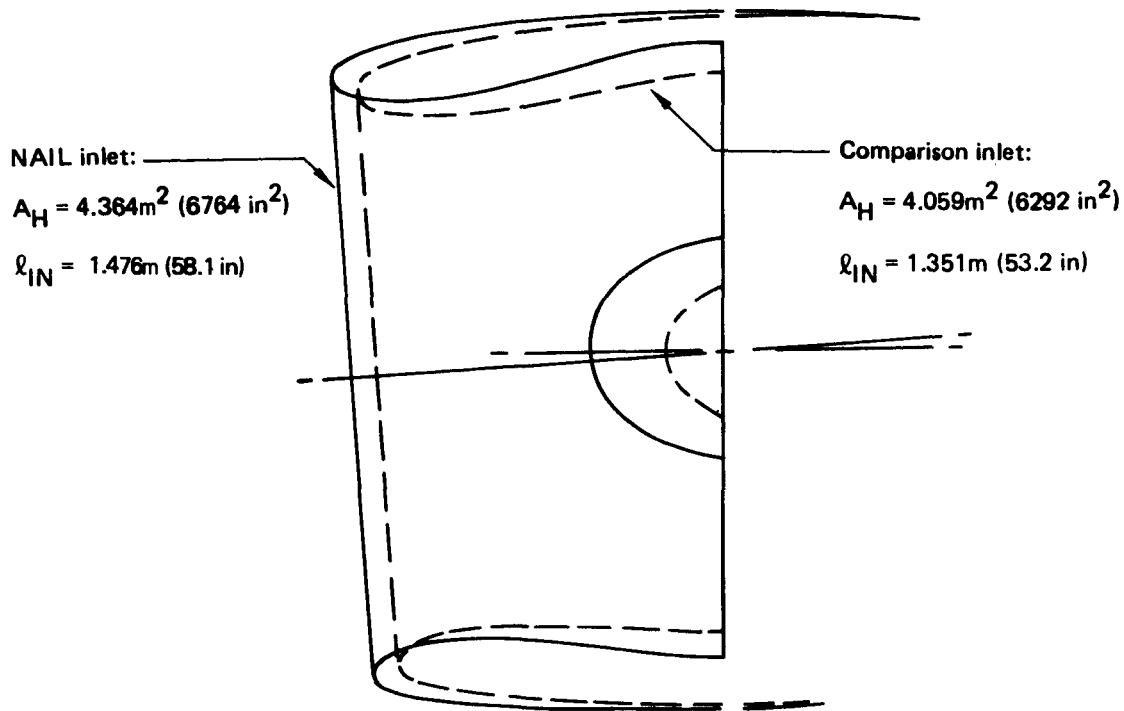Figure 33. Ruled Surface Fit to Pitching Moment Coefficient

49

NAIL inlet: ———————

$A_H = 4.364m^2$ (6764 in^2)

$\ell_{IN} = 1.476m$ (58.1 in)

Comparison inlet:

$A_H = 4.059m^2$ (6292 in^2)

$\ell_{IN} = 1.351m$ (53.2 in)

Figure 34. Inlet Profiles for Theoretical Load Comparison

There is a problem in the flow modeling that could affect C_{F_x} much more than it does C_{My}. Figure 36 shows a set of theoretical Cp distribution curves calculated for the NAIL inlet at the simulated high gross weight takeoff condition. Figure 37 shows the actual measured Cp's. The theoretical interior Cp's have converged to nearly the same value at the fan face. That is, there is only a weak pressure gradient from top to bottom of the inlet there. The test data show, however, that the lower surface is at about unity Cp lower than the top. The implication is that the streamlines in the inlet must be curved as indicated in figure 38, presumably as a result of boundary layer buildup (and perhaps a separation bubble) on the lower surface. Because the region where this discrepancy occurs is close to the A-flange, its moment arm is short, and it can produce a large change in F_x with only a slight effect on M_y.

It appears that inviscid aerodynamic theory alone is an inadequate tool for prediction of inlet airloads at takeoff or other high α_{IN} conditions. Satisfactory agreement awaits further development of viscous flow methods.
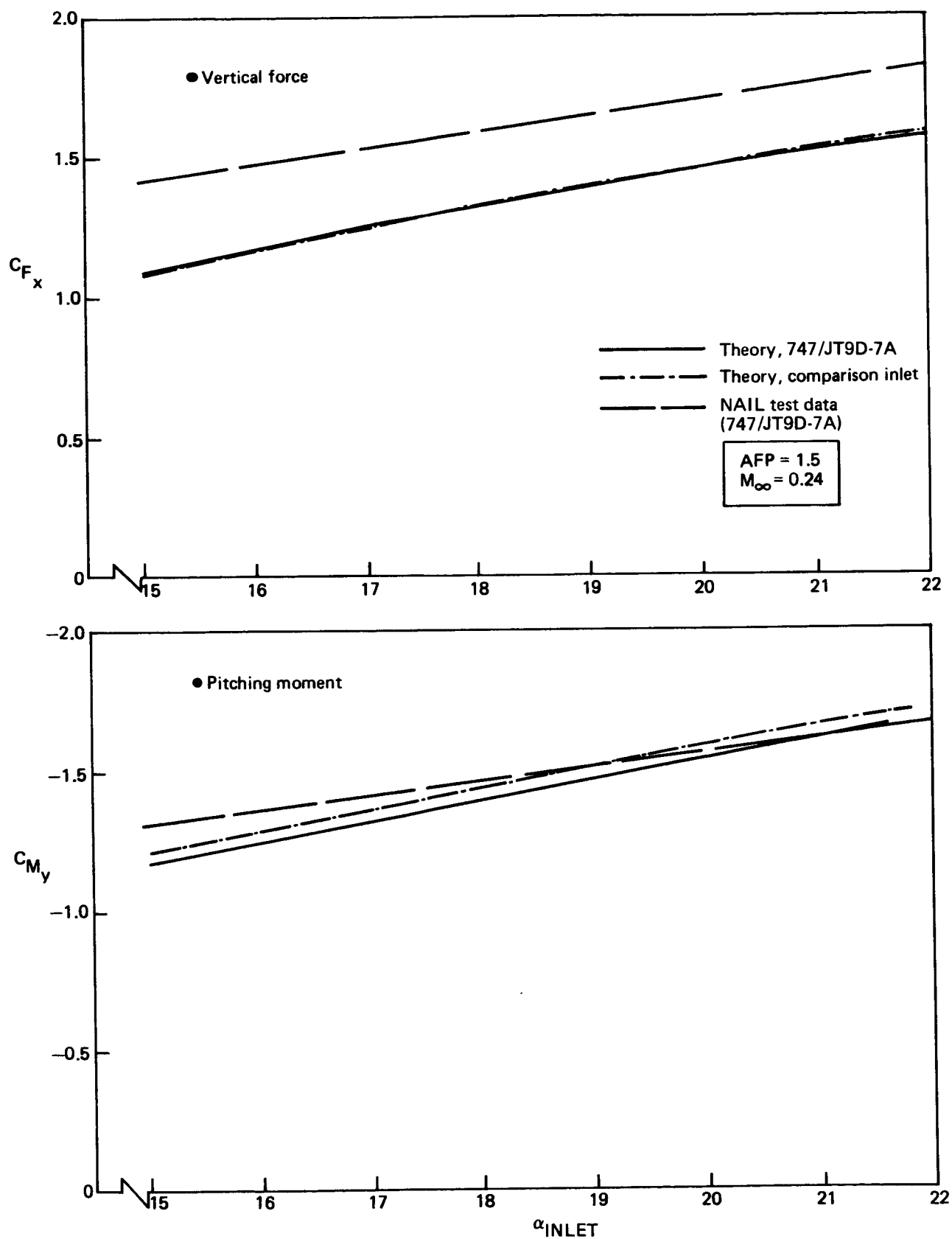
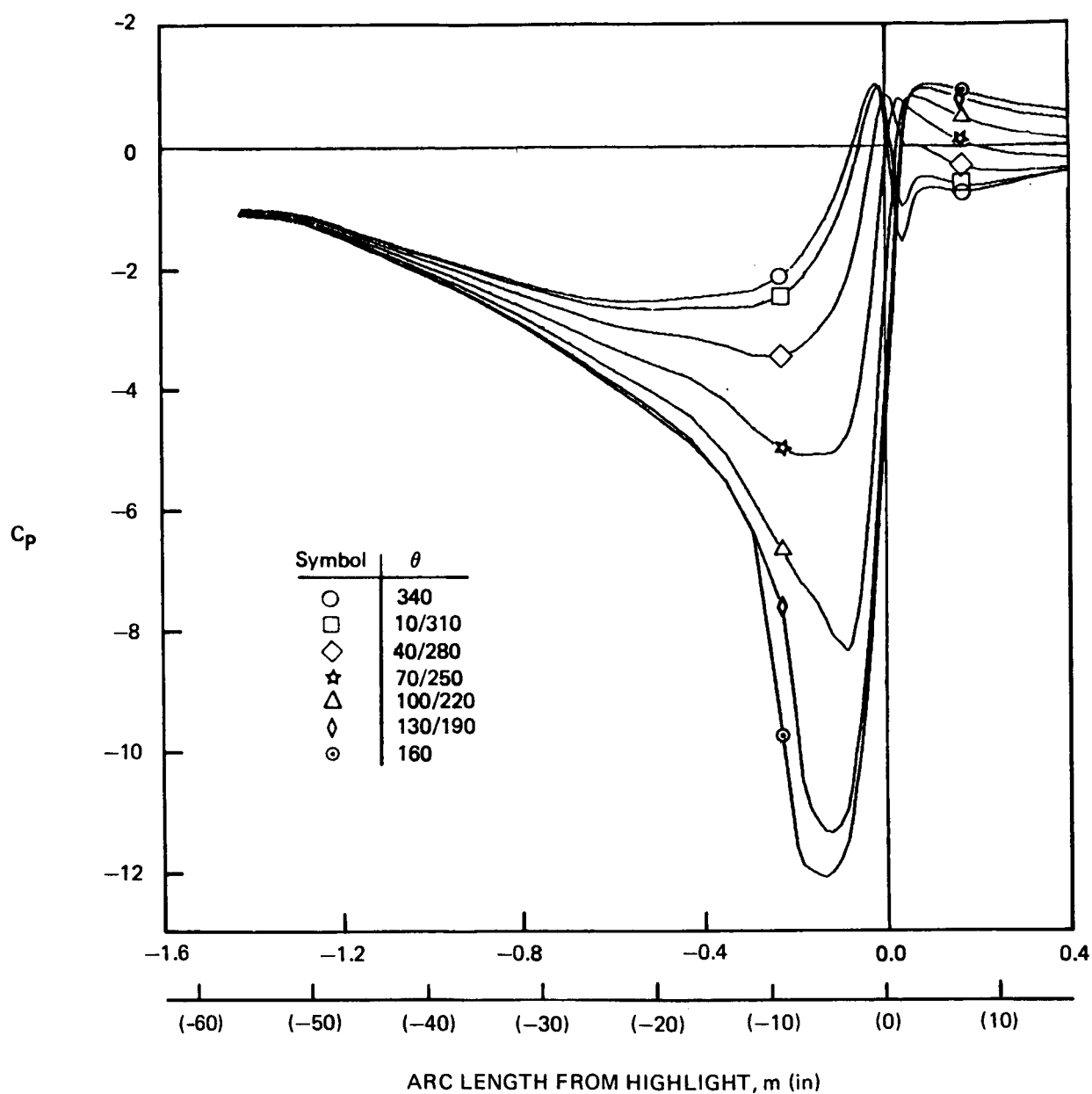*Figure 35. Comparison of Theoretical Airload Coefficients*

51

Symbol	θ
◯	340
☐	10/310
◇	40/280
☆	70/250
△	100/220
◊	130/190
⊙	160

ARC LENGTH FROM HIGHLIGHT, m (in)

Figure 36. Computed Pressures for High α_{IN}/AFP Condition

Symbol	θ
①	0
⊡	60
◇	120
⬙	180
△	240
⬗	300

Test 273-15
IRIG = 8:13:19.2

NOMINAL ARC LENGTH FROM INLET LIP, m (in)
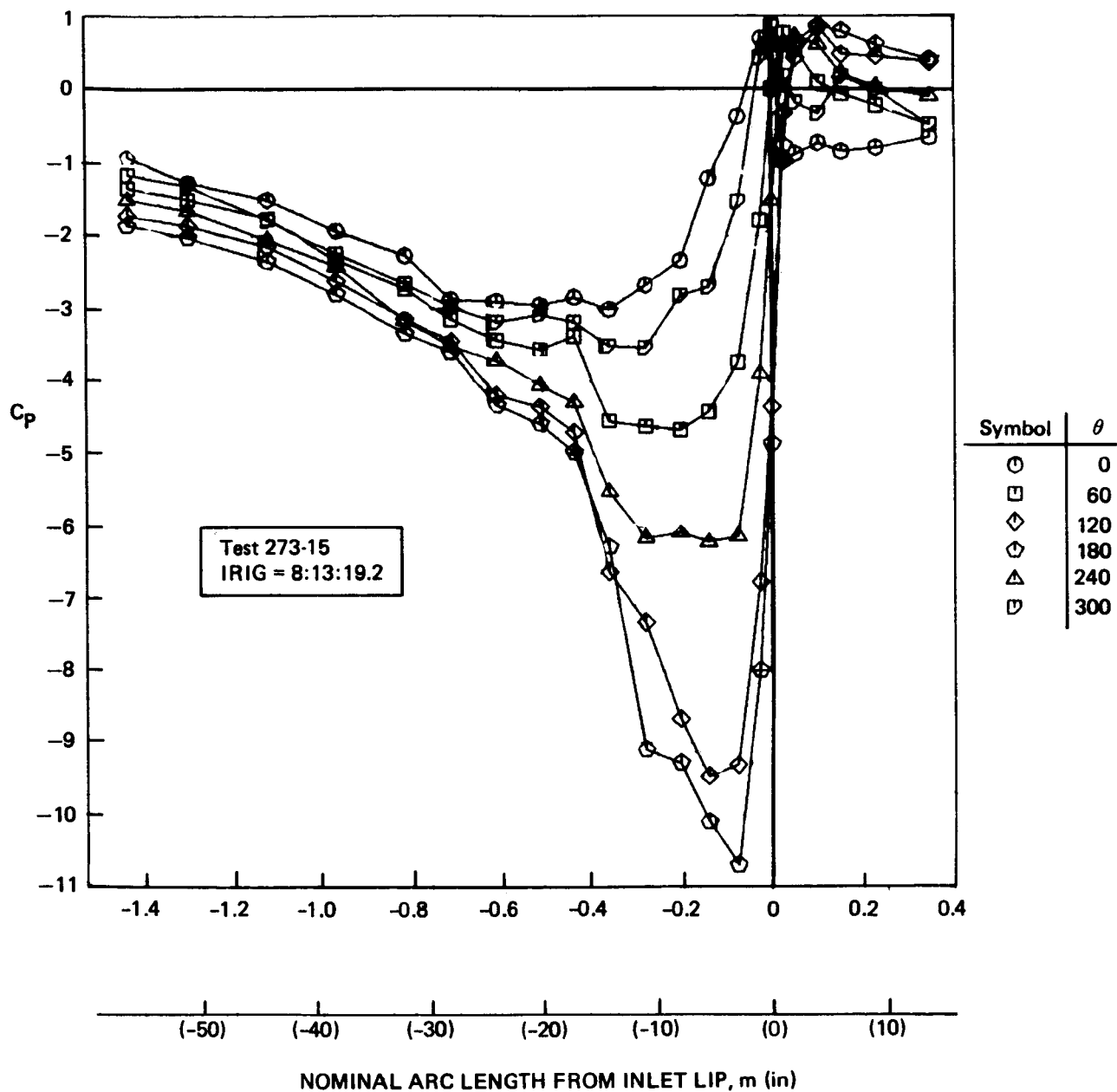
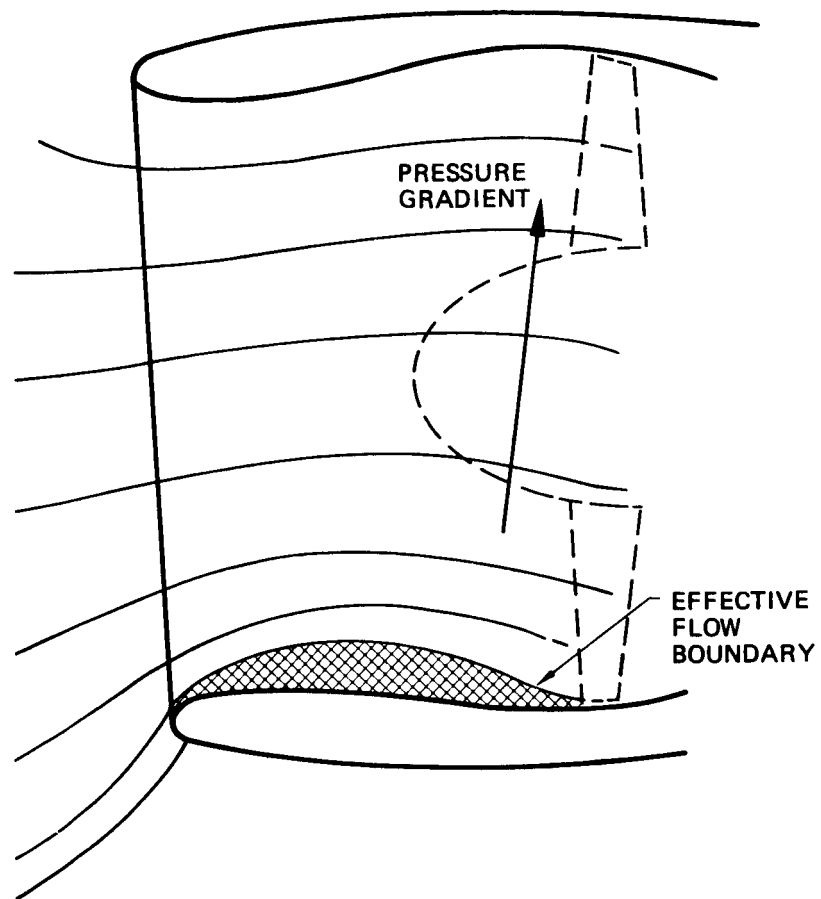Figure 37. Measured Engine 3 Inlet Pressures, High α_{IN}/AFP Condition

53

Figure 38. Pressure Gradient and Streamline Curvature

5.4 INERTIAL LOADS

Normal accelerations measured during takeoff and flight did not exceed 1.3g except during the high-g turn maneuvers. No significant turbulence was experienced during the NAIL program. For most flight conditions, the difference between g-loads measured at the airplane center of gravity and those measured on engines 3 and 4 was within the scatter of the data; i.e., the instruments responded only to steady-state accelerations of the whole airplane, experiencing no significant contributions from wing or nacelle flexible modes.

An exception to the steady-state accelerations occurred during a hard landing in test 273-15. The airplane landed at 313t (690 000 lb) gross weight with 135t (297 000 lb) of fuel and a sink rate of approximately 1.5 m/s (5 ft/s). Touchdown occurred at IRIG 8:20:49. Vertical acceleration at the airplane center of gravity was 1.53g, with peaks of 2g at engine 4 and 1.7g at engine 3. This case was selected for dynamic analysis. Another exception occurred during test 273-10, during which a mild gust was encountered at IRIG 12:11:52. Normal accelerations were 1.08g at the airplane center of gravity and 1.3g at the engines. Details of these cases are shown in the Appendix A of reference 5.

Pitch rates during takeoffs did not exceed 3 deg/s, and the peak value was achieved before reaching the maximum load factor.
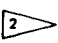
5.4.1 Inertial Data for NASTRAN Analyses

With six accelerometers on each engine, it was possible to calculate the six components of acceleration (three linear and three angular) at the engine's center of gravity. This was done for engine 3 both at the condition analysis times and at reference times selected to evaluate the influence of load changes on clearance changes. Schedules of inertial load components are given in tables 6 and 7.

5.4.2 Transient Inertial Loads

Significant transient loads occurred during the first landing in test 273-15. Pitch and vertical motion data for the engine 3 wing/strut intersection are shown in figures 39 and 40. These data were calculated from the six linear accelerations measured on the wing near the strut attachment points. Initial values of rates and displacements had to be assumed because direct measurements were not available. They were selected to give the known end values.

The measured accelerations were considerably lower than those computed for a 3 m/s (10 ft/s) landing at 222t (490 000 lb) gross weight in reference 3. This is consistent with the inferred initial sink rate of 1.5 m/s (5 ft/s), although onboard observers reported that the landing felt very hard. (The actual landing weight was 313t 690 000 lb , somewhat higher than the 747's design maximum landing weight of 256t [564 000 lb].)
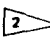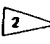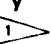
55

Table 6. Engine 3 Inertial Data
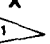
Test no.	Condition	IRIG hr/min/sec	Acceleration Axial A_z [1]	Acceleration Side A_y [1]	Acceleration Vertical A_x [1]	Pitch rate [2]	Yaw rate [2]
273-7	101	6:41:36	−0.25	−0.10	1.0	−0.40	−0.30
273-7		6:41:44	−0.30	−0.15	1.08	0.40	−0.10
273-10	101	9:44:02	−0.23	−0.30	1.0	−0.3	0
		9:44:10	−0.40	−0.20	1.15	1.60	−0.30
273-11	101	10:13:46	−0.20	−0.25	1.0	0	−0.1
		10:13:52	−0.40	−0.30	1.2	1.24	0.65
273-15	118	8:12:15	−0.20	−0.20	1.0	0	0
273-15		8:12:24	−0.35	−0.20	1.1	1.0	0
273-15		8:13:16	−0.30	−0.20	1.1	1.49	0.1
		8:13:18	−0.35	−0.10	1.2	1.98	0.24
273-10	102	9:45:59	−0.28	−0.15	0.955	−0.60	−0.70
273-7	103	7:28:44	NDA	−0.1	0.95	−0.5	−0.26
273-7	104	7:49:26	NDA	−0.1	0.98	−0.25	−0.13
273-7	105	7:56:40	NDA	−0.1	0.98	−0.25	−0.18
273-15	106	12:09:26	−0.07	−0.15	0.99	−0.53	−0.20
273-7	107	8:12:53	NDA	−0.1	1.04	−0.24	−0.18
273-15	108	11:39:00	−0.09	−0.20	0.60	−1.9	0.10
273-7	109	8:18:58	NDA	−0.1	0.91	−0.20	−0.37
273-7	110	8:22:04	NDA	0.1	1.05	0.10	−0.06
273-7	110	8:22:26	NDA	−0.1	1.24	0.37	−0.25
273-7	111	8:24:52	NDA	−0.12	0.91	−0.74	−0.49
273-7	112	8:28:56	NDA	−0.1	1.04	0	−0.18
273-7	113	8:34:27	NDA	−0.1	0.961	−0.73	−1.64
273-7	114.1	8:40:36	NDA	−0.1	1.1	0.5	−0.24
273-7	115	8:45:59	NDA	−0.15	1.02	−0.5	0
273-10	116	13:33:37	−0.19	−0.40	1.45	3.0	−2.2
273-10		13:33:58	−0.27	−0.25	1.98	3.99	−1.8
273-10	117	13:40:30	−0.10	−0.30	1.07	0	−0.25
273-10		13:41:07	−0.25	−0.40	1.60	6.49	−3.9
273-15	120	11:03:40	−0.14	−0.17	1.3	1.77	2.3
273-15		11:04:03	−0.25	−0.30	1.98	5.13	3.4
273-15	121	11:06:48	−0.15	−0.15	1.1	0.97	3.1
273-15		11:07:25	−0.25	−0.20	1.57	6.70	5.2
273-10	123	13:26:17	−0.35	−0.1	1.27	5.6	5.5

● Acceleration coordinates: nacelle axes, figure 18
● Pitch rate: positive noseup
● Yaw rate: positive right turn
● NDA: accelerometer failed to operate properly

[1] g

[2] deg/sec

56

Table 7. Engine 4 Inertial Data

Test no.	Condition	IRIG hr/min/sec	Acceleration Axial A_z [1]	Acceleration Side A_y [1]	Acceleration Vertical A_x [1]	Pitch rate [2]	Yaw rate [2]
273-7	101	6:41:44	−0.25	−0.15	1.08	0.40	−0.10
273-10	101	9:44:10	−0.1	−0.50	1.15	1.60	−0.30
273-11	101	10:13:52	−0.20	−0.20	1.1	1.24	0.65
273-15	118	8:13:18	−0.25	−0.20	1.1	1.98	0.24
273-10	102	9:45:59	−0.15	−0.10	1.15	−0.60	−0.70
273-7	103	7:28:44	NDA	−0.1	0.95	−0.5	−0.26
273-7	104	7:49:26	NDA	−0.1	0.98	−0.25	−0.13
273-7	105	7:56:40	NDA	−0.1	0.98	−0.25	−0.18
273-15	106	12:09:26	0.05	−0.10	0.95	−0.53	−0.20
273-7	107	8:12:53	NDA	−0.1	1.04	−0.24	−0.18
273-15	108	11:39:00	0.05	0	0.60	−1.9	0.10
273-7	109	8:18:58	NDA	−0.1	0.91	−0.20	−0.37
273 7	110	8:22:26	NDA	−0.1	1.24	0.37	−0.25
273-7	111	8:24:52	NDA	−0.12	0.91	−0.74	−0.49
273-7	112	8:28:56	NDA	−0.1	1.04	0	−0.18
273-7	113	8:34:27	NDA	−0.1	0.961	−0.73	−1.64
273-7	114.1	8:40:36	NDA	−0.1	1.1	0.5	−0.24
273-7	115	8:45:59	NDA	−0.15	1.02	−0.5	0
273-10	116	13:33:58	−0.10	−0.40	1.90	3.99	−1.8
273-10	117	13:41:07	−0.15	−0.30	1.50	6.49	−3.9
273-15	120	11:04:03	−0.10	−0.30	1.95	5.13	3.4
273-15	121	11:07:25	−0.20	−0.15	1.5	6.70	5.2
273-10	123	13:26:17	−0.25	−0.10	1.15	5.6	5.5

● Acceleration coordinates: nacelle axes, figure 18

● Pitch rate: positive noseup

● Yaw rate: positive right turn

●NDA: accelerometer failed to operate properly

[1] g

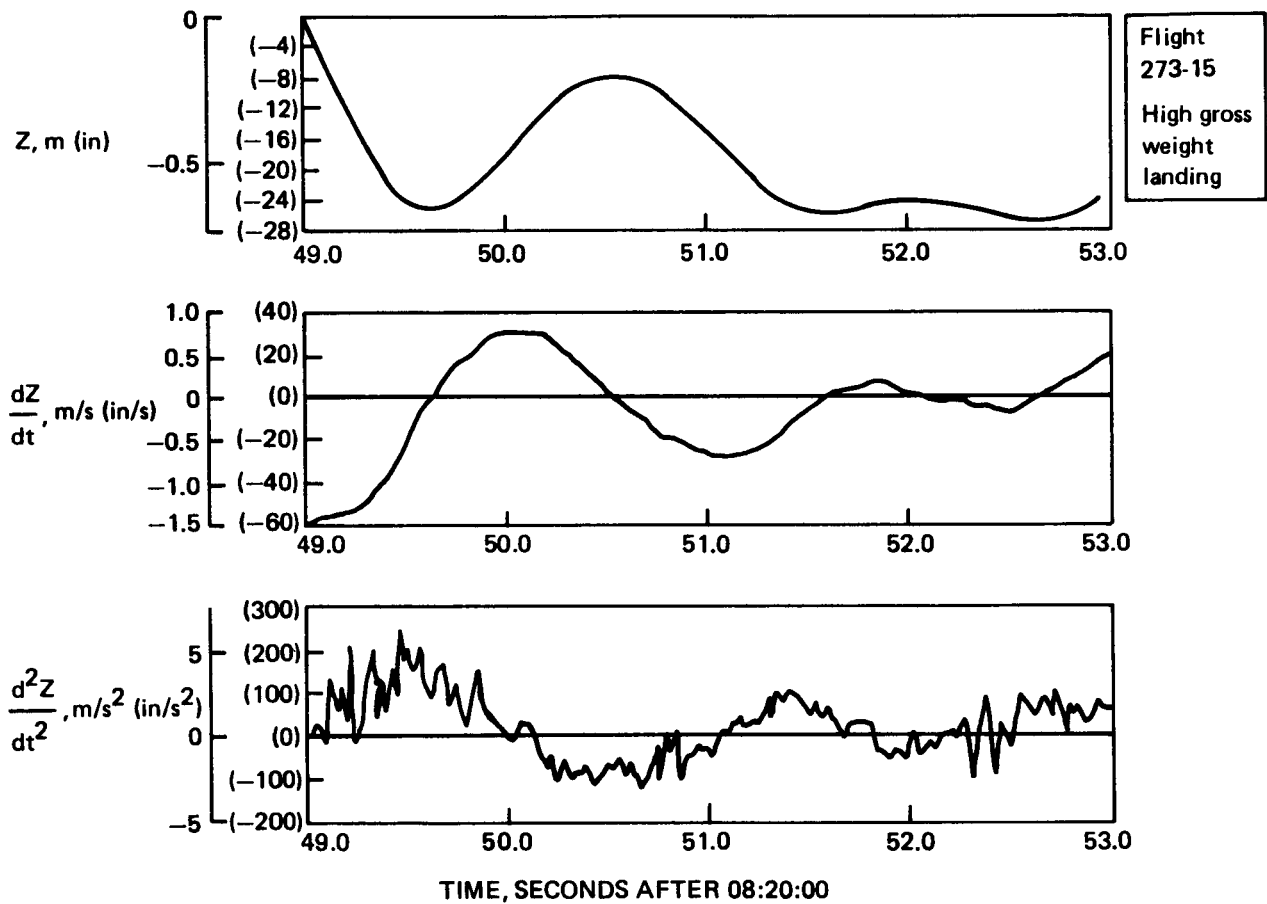[2] deg/sec

57

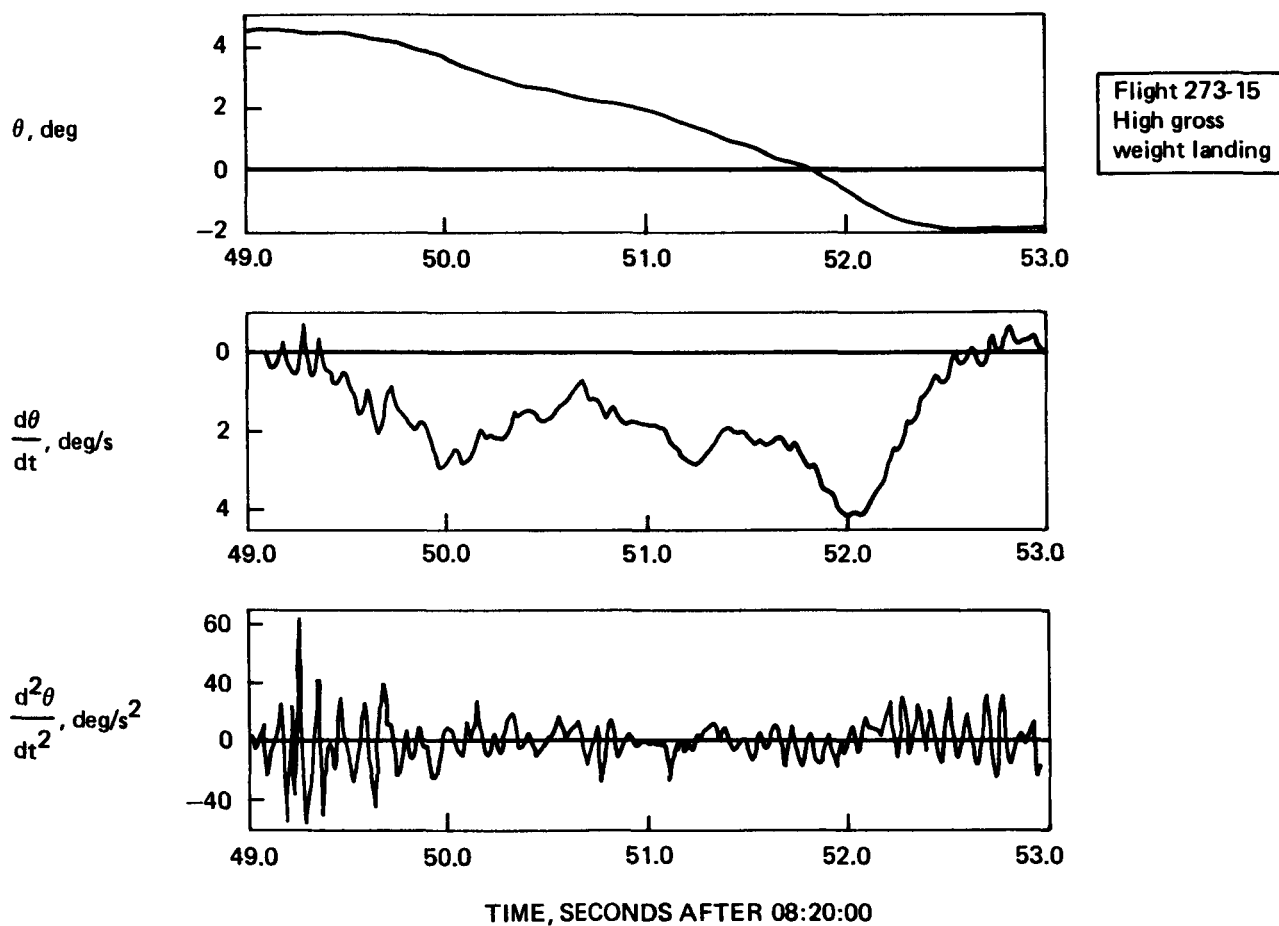Figure 39. Vertical Motion at Strut/Wing Interface, Engine 3

58

Figure 40. Pitch Motion at Strut/Wing Interface, Engine 3

6.0 CONCLUSIONS AND RECOMMENDATIONS

6.1 CONCLUSIONS

6.1.1 Management

The NAIL program was a highly successful program that had an unusual management structure: sponsorship by two different NASA research centers with execution by two distinct industrial organizations. Despite the apparent complexity of this arrangement, planned objectives were met or exceeded, on time and within budget.

6.1.2 Technical

The airloads measured in the takeoff phase of flight were higher than anticipated. Some other phases, specifically the stall warning maneuvers, generated less severe loads than those estimated in earlier analyses (ref. 3) because the flight techniques differed from those that had been assumed.

Inertial loads were less severe than previous studies had indicated.

Inlet angle of attack and engine airflow together determine inlet airloads. Inlet angle of attack can be influenced by the pilot through three parameters: flap setting, airspeed, and load factor (g). Airflow is determined by power setting. It may be possible to reduce operating airloads significantly by suitable revisions to flight procedures.

The airload data developed in the NAIL program will be applicable in nondimensional form to underwing high-bypass ratio turbofan installations involving other airplane and engine combinations than the JT9D-7/Boeing 747.

A data base has been established that will permit evaluation and verification of improved analytical methods for studying aerodynamic interactions between wings and propulsion systems for turbofan-powered subsonic transport aircraft.

6.2 RECOMMENDATIONS

6.2.1 Management

The combined center management approach should be considered by NASA whenever the problem under investigation cuts across technology lines, as in this case, engine/airframe.

6.2.2 Technical

It is suggested that modifications to flight procedures be considered with a view to reducing high-load occurrences in both test (acceptance flights) and airline service. In acceptance flights, recovery from stall warning maneuvers can result in lower load levels if adding power is postponed. (This is feasible because the altitude loss under those conditions is not a problem.) In airline service, use of a 20-deg flap setting for takeoff and postponement of takeoff rotation to a higher speed will tend to reduce the maximum inlet angle of attack attained, resulting in significant airload reductions.

The loads data obtained in the NAIL program should now be used in formulating design criteria for engine-related structures to ensure minimum fuel economy degradation from the start of the design process.

6.2.3 Future Work

More data are needed on the statistical aspects of engine loads. The NAIL program developed no information on the takeoff rotation speeds, flap setting selections, or rotation load factors normally encountered in airline service. Such data would be helpful in the use of the aerodynamic data gained by NAIL on subsequent design efforts. It is recommended that NASA develop a statistically significant data base as part of its ongoing flight loads measurement program.

7.0 REFERENCES

1. Pratt & Whitney Aircraft Group. Performance Deterioration Due to Acceptance Testing and Flight Loads, NASA CR 165572, 1981.

2. Pratt & Whitney Aircraft Group and Boeing Commercial Airplane Company. B747/JT9D—Flight Loads and their Effect on Engine Running Clearances and Performance Deterioration, NASA CR 165573, 1981.

3. Jay, A. and Todd, E. S. Effect of Steady Flight Loads on JT9D-7 Performance Deterioration. NASA CR 135407, 1978.

4. Sallee, G. P. and Martin, R. L. Expanded Study of Feasibility of Measuring In-Flight 747/JT9D Loads, Performance, Clearance, and Thermal Data, NASA CR 159717, 1980.

5. Boeing Commercial Airplane Company. Nacelle Aerodynamic and Inertial Loads (NAIL) Project Test Report, NASA CR 165760, 1981.

6. Press, Harry and Steiner, Roy. An Approach to the Problem of Estimating Severe and Repeated Gust Loads for Missile Operations, NACA TN 4332, 1958.

1. Report No. NASA CR 165807	2. Government Accession No. -	3. Recipient's Catalog No. -
4. Title and Subtitle NACELLE AERODYNAMIC AND INTERTIAL LOADS (NAIL) PROJECT, FINAL TECHNICAL REPORT		5. Report Date March 1982
		6. Performing Organization Code -
7. Author(s) Preliminary Design Department Boeing Commercial Airplane Company (BCAC)		8. Performing Organization Report No. D6-49360
		10. Work Unit No. -
9. Performing Organization Name and Address Boeing Commercial Airplane Company (BCAC) P.O. Box 3707 Seattle, WA 98124		11. Contract or Grant No. NAS1-15325
		13. Type of Report and Period Covered Contractor report
12. Sponsoring Agency Name and Address National Aeronautics and Space Administration Washington, DC 20546		14. Sponsoring Agency Code -

15. Supplementary Notes

Technical monitor: D. B. Middleton
NASA-Langley Research Center

16. Abstract

A flight test survey of pressures measured on wing, pylon, and nacelle surfaces and of the operating loads on Boeing 747/Pratt & Whitney JT9D-7A nacelles was made to provide information on airflow patterns surrounding the propulsion system installations and to clarify processes responsible for inservice deterioration of fuel economy.

Inlet airloads were measured by integration of pressures recorded at 252 locations on the right-hand inboard nacelle. Pressures also were recorded at 45 locations on the right-hand outboard nacelle for comparison. Inertial loads were measured on both nacelles using accelerometers and rate gyros. Flight conditions included takeoffs at several gross weights, high-g turns, and a simulated acceptance flight.

Airloads at takeoff rotation were found to be larger than at any other normal service condition because of the combined effects of high angle of attack and high engine airflow. Inertial loads were smaller than previous estimates had indicated.

A procedure is given for estimating inlet airloads at low speeds and high angles of attack for any underwing high bypass ratio turbofan installation approximately resembling the one tested. Flight procedure modifications are suggested that may result in better fuel economy retention in service.

Pressures were recorded on the core cowls and pylons of both engine installations and on adjacent wing surfaces for use in development of computer codes for analysis of installed propulsion system aerodynamic drag interference effects.

17. Key Words (Suggested by Author(s)) Fuel economy Inlet airloads Inertial loads Nacelle Turbofan	18. Distribution Statement
19. Security Classif. (of this report) Unclassified	20. Security Classif. (of this page) Unclassified	21. No. of Pages 67	22. Price

N 305